# Tectonically- and climatically-driven mountain-hopping erosion in Central Guatemala from detrital $^{10}$Be and river profile analysis

Gilles Y Brocard[1], Jane K Willenbring[2], Tristan Salles[3], Michael Cosca[4], Axel Guttiérez-Orrego[5], Noé Cacao Chiquín[5], Sergio Morán-Ical[5], Christian Teyssier[6]

[1]Archéorient, University of Lyon 2, 69365 Lyon, France

[2] Department of Geological Sciences, Stanford University, Stanford, CA 94305, USA

[3]: School of Geosciences, University of Sydney, Camperdown, Australia

[4]: U.S. Geological Survey, Denver Federal Center, Denver, CO 80225, USA

[5]: Carrera de Geología, Universitad San Carlos de Guatemala, Centro Universitario del Noreste, 16001 Cobán, Guatemala.

[6]: Department of Earth Sciences, University of Minnesota, Minneapolis MN 55455, USA

*Correspondence to*: Gilles Brocard (gilles.brocard@mom.fr)

**Abstract.** The rise of a mountain range affects moisture circulation in the atmosphere and water runoff across the land surface, modifying the distribution of precipitation and ~~the shape of~~ drainage patterns. Water routing in turn affects erosion on hillslopes and incision in river channels. The rise of a mountain range thereby alters the erosion of surrounding mountain ranges. We document here such influence in Central Guatemala, where two parallel, closely spaced mountain ranges formed during two consecutive pulses of single-stepped uplift, one from 12 to 7 Ma (Sierra de Chuacús-Sierra de las Minas), and the second one after 7 Ma (Altos de Cuchumatanes). We explore the climatic and tectonic processes by which the rise of the most recent range drove the slowing of river incision and hillslope erosion over the previously-uplifted range. $^{40}$Ar-$^{39}$Ar dating of perched volcanic deposits documents the sequential rise and incision of the two mountain ranges. Terrestrial cosmogenic $^{10}$Be in river sediments shows that hillslopes in the older range today erode more slowly than in the younger range (20-150 vs. 300 m·My$^{-1}$), and that these differences mimic the current distribution of precipitation, the younger range intercepting the atmospheric moisture before it reaches the older range. River channel steepness and deformation of paleovalleys in the new range further show that the younger has risen faster than the older range up to today. We review how atmospheric moisture interception and river long-profile adjustment to the rise of the new range contribute to the decrease in erosion rates over the old range. We then explore how the topography of the older range has evolved in response to the decrease in erosion rates. The old range undergoes topographic decay, owing to the stalling of river incision

around its base. Aridification makes such decay very slow, and dominated by backwearing, rather than downwearing, marked by the stacking of slowly-migrating erosion waves along the mountain flanks, and by the formation of pediments around its base. The morphology of the old range is therefore transitioning from that of a front range to that of a dry interior range.

## 1. Introduction

The relief of mountain ranges affects the circulation of moisture in the atmosphere and of precipitated water across the land surface. Moisture precipitates on the windward side of mountains and rain shadows are cast over their lee-side, and beyond on downwind reliefs (e.g.Meijers et al., 2018; Galewsky, 2009). Overland flow generates hillslope erosion and river incision. River drainages are dynamic systems that transmit downstream disturbances that affect their headwaters, and also transmit upstream disturbances affecting their downstream reaches, in particular the adjustment of river profiles to the rise of mountain ranges (Humphrey and Heller, 1995; Whittaker and Boulton, 2012). Signals are then transmitted from the rivers to the toe of valley slopes, and then uphill along valley slopes (Harvey, 2002; Mudd and Furbish, 2007). Through this combination of top-down (precipitation and runoff) and bottom-up (upstream-migrating signals) processes, the rise of a mountain affects the erosion of surrounding reliefs.

The growth of contractional orogens commonly involves outward, sequential propagation of contraction. Moisture, on the other hand, is often advected from the foreland toward the orogen interior. Precipitated water is then commonly returned to the foreland along river networks that flow from the interior to the foreland. In such setting, the in-sequence rise of frontal ranges, at the margins of orogens, will therefore frequently occur both upwind and downstream of pre-existing reliefs (Garcia-Castellanos, 2007). The rise of a new frontal range therefore leads to the aridification of previously uplifted ones. In the meantime, the new frontal range rises across the course of rivers that flow from the interior to the foreland. It will impart the steepening of rivers transverse to the range (Leland et al., 1998), thereby promoting a transient decreases in river incision rates farther upstream (Champel et al., 2002). It may spark the reorganization of the range-transverse river network (Jackson et al., 2002; van der Beek et al., 2002). In some cases, topography and tectonic structure will adapt fast enough to re-establish a new equilibrium relief, equilibrium climate, and equilibrium tectonic structure (Willett and Brandon, 2002; Whipple and Meade, 2006). In other cases, the slowing down of the landscape response, upstream and downwind or a rising range, as a result of aridification, will lead to the disintegration of river drainages, following by the topographic decay of the interior ranges, an evolution conducive to the nucleation and growth of orogenic plateaus (Sobel et al., 2003; Garcia-Castellanos, 2007). These two evolutionary pathways have been explored at the scale of entire orogens, but they are less frequently documented at the scale of individual mountain ranges, where the hallmark of these evolutions interferes with

more local signals resulting from spatial variations in bedrock erodibility, topographic inheritances, or stochastic processes such as landslides.

We document here the effects of the rise of a recent mountain range (the 170 km-long Altos de Cuchumatanes, or AC range) on the evolution of an older range (the 220 km-long Sierra de Chuacús-Sierra de las Minas, or SC-SM range) in Guatemala (Fig.1). Sharp topographic, climatic, and tectonic gradients affect this relatively small (350 x 100 km) area, allowing us to conduct detailed investigation of the interactions between the two ranges. The SC-SM range grew first; its flanks were deeply eroded in late Miocene time (Brocard et al., 2011). The AC range started to grow at the end of the late Miocene, next to the SC-SM range. The rise of the AC range sparked widespread drainage rearrangement in front of the SC-SM, characterized by numerous river captures (Brocard et al., 2011). These captures, however, did not generate upstream-migrating waves of accelerated erosion. Instead, river incision almost completely stalled upstream of the capture sites (Brocard et al., 2011). We investigate here the processes that arrested river incision, and retrieve from the characteristics of their river long-profiles some insights on how arrested incision affected the evolution of these ranges.

New $^{40}Ar/^{39}Ar$ ages on volcanic rocks first help us to tighten the chronology of river incision and surface uplift in the SC-SM range. Detrital terrestrial $^{10}Be$ erosion rates provide a snapshot of current spatial variations of erosion rates across the study area. Profile linearization is implemented to study the complex long-profiles of the rivers that drain these two ranges. River knickpoints are then carefully classified in order to extract river knickpoints that inform long-term landscape dynamics and the response time of river incision to the sequential uplift of the two ranges. We then discuss successively the contribution of topographically-controlled climate and of river profile adjustment to the observed decrease in incision rates in the SC range during the rise of the AC range. We then discuss how both processes contribute to the overall decrease in erosion over the SC range, and to the slowing down of migrating knickpoints. We finally present some topographic characteristics that appear as direct consequences of the slowing down of erosion over the older range.

## 2. Origin and evolution of the mountain ranges of Central Guatemala

### 2 .1. Tectonics and orogenesis

Left-lateral motion along the North American-Caribbean plate boundary has produced elongate ranges parallel to the plate boundary in Central Guatemala (Fig.1a). We investigate here the growth and erosion of two of these ranges (Fig.1b). Rocks in the SC-SM range display a deeply penetrative, sub-vertical tectonic fabric, imparted by 70 My of left-lateral wrenching along the Caribbean-North American plate boundary (Ratschbacher et al., 2009; Ortega-Gutierrez et al., 2004; Ortega-Obregón et al., 2008). Since Eocene times, left-lateral motion between the Caribbean and North American plates has been accommodated mostly by the Motagua fault, and, to a lesser extent, by the Polochic fault (Fig.2b). The Motagua fault is,

with >1,100 km of total cumulative offset, the active subaerial fault with the largest cumulative offset on Earth. The Polochic fault has a total offset 125 ± 5 km (Burkart, 1978). The Polochic fault probably branches out of the Motagua fault offshore, somewhere in the Caribbean Sea (Fig.1a), before running on land at an average distance of 50 km from the Motagua fault. Strain along the plate boundary is strongly partitioned between almost pure left-lateral slip on the Motagua and Polochic faults and boundary-normal dip-slip on faults parallel to the Polochic and Motagua faults (Authemayou et al., 2011b; Brocard et al., 2012).

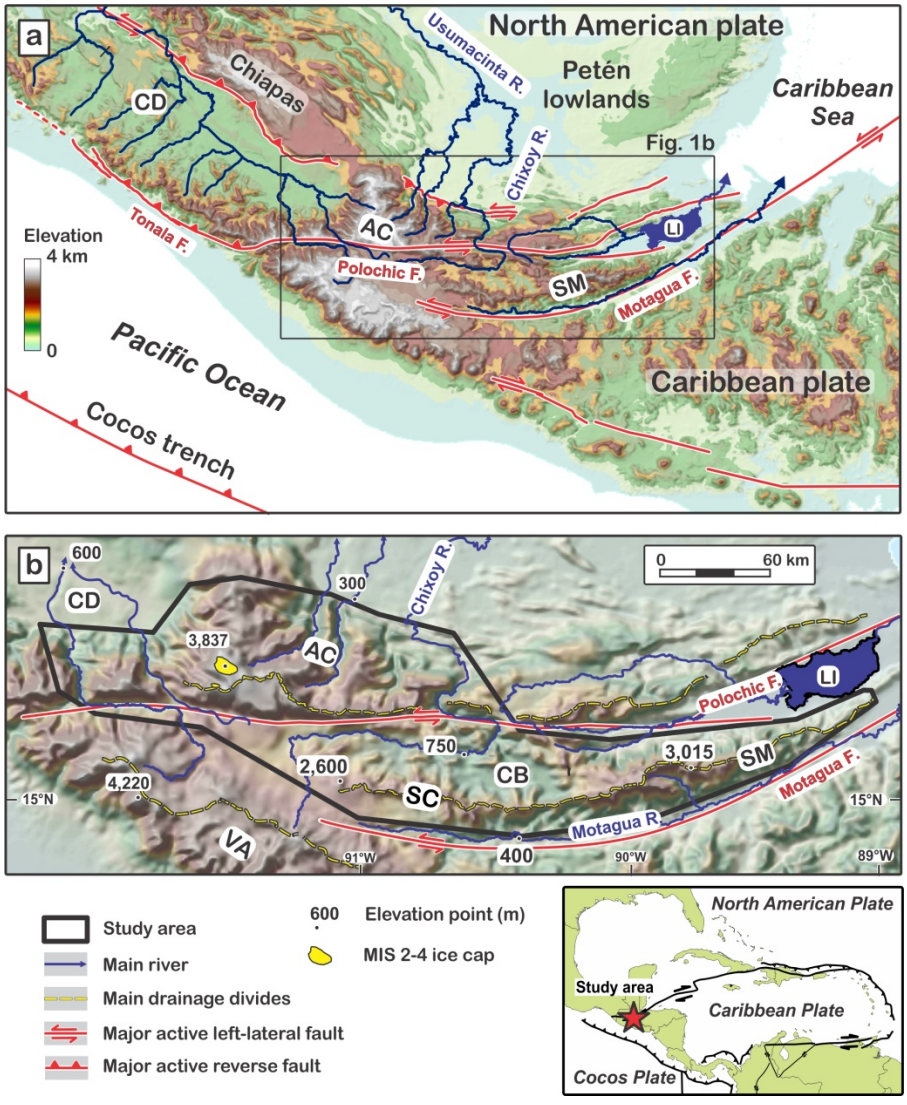

Figure 1. Shaded topography of the study area, showing the tectonic setting of Central Guatemala in general (a), and of the studied range specifically (b).Topographic features: CB: Chixóy River basin, CD: Central Depression of Chiapas, AC: Altos de Cuchumatanes (AC range), LI: Lake Izabal, SC: Sierra de Chuacús (SC range), SM: Sierra de las Minas (SM range), VA: Central American Volcanic Arc. MIS: $\delta^{18}O$ Marine Isotopic Stage

Today, Central Guatemala is straddled by 3-4 km-high ranges that separate deep valleys with floors stand at elevations as low as 0.2-0.8 km (Fig.1b). In Middle Miocene times, however, the topography of Central Guatemala was much more subdued. Remnants of that past topography (referred to as the Maya surface (Brocard et al., 2011)) still cap numerous mountaintops across the study area (Fig.2). They are separated by regions where the Maya surface has been deeply incised (Fig.3). The low Miocene relief formed from the topographic decay of Eocene folds (Authemayou et al., 2011b; Brocard et al., 2011). It grades to the east and north into lowlands, near the Caribbean Sea, indicating that it formed near sea level. Its uplift started after the Middle Miocene, then affecting both the southern (Simon-Labric et al., 2013), and northern side of the Motagua fault, as far north as the Polochic fault (Brocard et al., 2011). Uplift led the rise of the SC-SM range during the late Miocene. Valleys up to 1,000 m deep were incised within its northern flank between 12 to 7 Ma (Brocard et al., 2011).

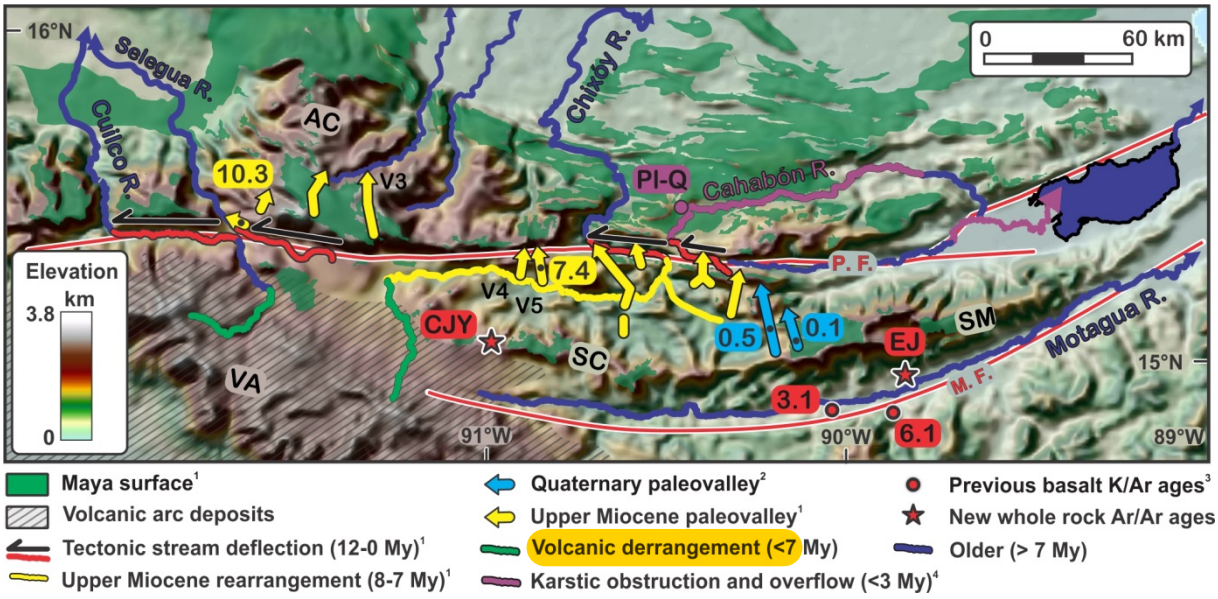


Figure 2. Age of geomorphic markers and drainage lines. Ages of Miocene valleys and Quaternary paleovalleys (V1-V12) provided in My. Data source: 1: (Brocard et al., 2011), 2: (Brocard et al., 2012), 3: (Tobisch, 1986), 4: Plio-Quaternary lacustrine deposits (Brocard et al.,

2015a). Newly dated lavas: CJY: Chujuyúb, EJ: El Jute. Range names: AC: Altos de Cuchumatanes, SC: Sierra de Chuacús, SM: Sierra de las Minas, VA: volcanic arc. Faults: MF: Motagua, PF: Polochic. Background: shaded GTOPO 30 DEM.

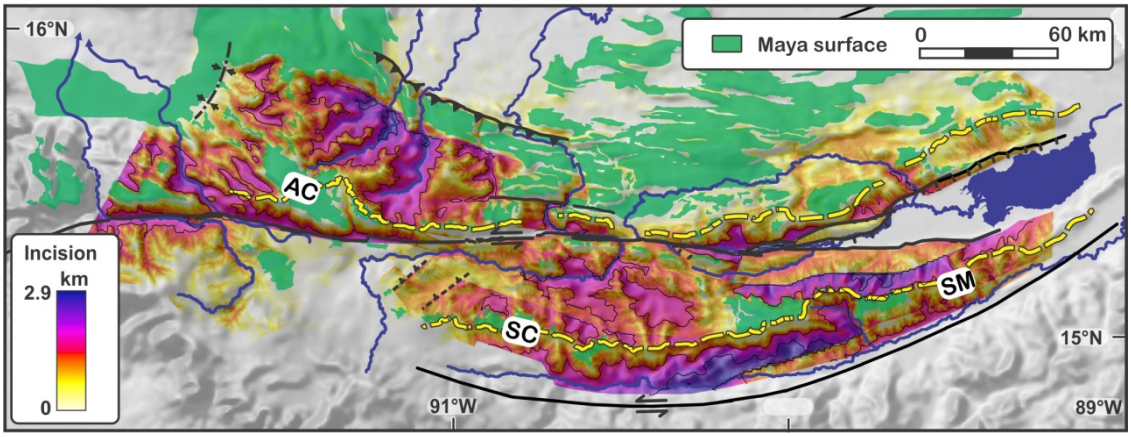


Figure 3. Incision below the Middle Miocene Maya surface, based on the elevation of surface remnants (upland relict surface). Incision contour line spacing: 1km. Yellow dashed lines: range drainage divides .AC: Altos de Cuchumatanes, SC: Sierra de Chuacús, SM: Sierra de las Minas, VA: volcanic arc.

Uplift propagated north of the Polochic fault during the Late Miocene (Brocard et al., 2011). It was marked by the rise of the AC range in response to contraction in the North American plate (Authemayou et al., 2011a). The rise of the AC range drove widespread reorganization of the river network that drains the northern flank of the SC-SM range (Fig. 2). Numerous river valleys were then abandoned and were left stranded on the rising AC range. Their deformation indicates that the AC range has risen >1-2 km relative to the SC range over the past 7 My (Brocard et al., 2011). Earthquake focal mechanisms further indicate that the tectonic structures bordering the AC range to the north still accommodates shortening today (Guzmán-Speziale, 2010; Authemayou et al., 2011b).

While contraction has defined the evolution of the western part of the study area, transtension has prevailed further east since at least the Late Miocene. Such dominance of transtension in the east results chiefly from an eastward increase in the divergence angle between the strike of the plate boundary and the direction of plate motion (Rogers and Mann, 2007). Transtension led to development of the Lake Izabal basin (Fig.1a) into which ~5 km of terrigenous sediments have accumulated since the Middle Miocene (Carballo-Hernandez et al., 1988; Bartole et al., 2019). Transtension also led the growth of another ≥1.4 km-deep, elongate (125x15 km) sedimentary basin at the eastern termination of the subaerial trace of the Motagua fault, next to the Caribbean Sea (Carballo-Hernandez et al., 1988). Transtension spread further to the west

during the Pliocene, generating still-active normal faults that disrupt the northern flank of the SM range (Authemayou et al., 2011b; Brocard et al., 2012).

### 2.2. Drainage evolution since the Middle Miocene

The rivers that drain the northern flank of the SC range represent the headwaters of a network that, farther downstream, experienced widespread reorganization during the late Miocene (Fig.2). Reorganization led to the formation of range-parallel rivers between the SC-SM and the AC ranges that collect the rivers that drain the northern flank of the SC-SM range and funnel them into the Chixóy River, one of the few rivers (together with the Cahabón, Chixóy, Selegua, and Cuilco Rivers, Fig.2), that still crosses the AC range. These rivers that cross the AC range also cross the trace of left-lateral Polochic fault, before entering the AC range. The Polochic fault has deflected and lengthened the course of the rivers that cross its trace (Fig.2) since the late Miocene (Brocard et al., 2011). Transtensional faulting along the northern flank of the SM range has initiated a second and still ongoing pulse of drainage reorganization during the Quaternary (Fig.2) (Brocard et al., 2012).
Large volcanoclastic aprons have piled up along the NE flank of the Central American Volcanic arc since the Pliocene. They have buried the western end of the SC range, deranging its river network. This complex area is therefore excluded from the present study. Likewise, the karstic highlands of Central Guatemala, especially those located north of the Polochic fault are also excluded from the analysis, their dynamics is mostly under the influence of the higher-frequency opening and closure of subterranean karstic pathways (Brocard et al., 2015a; Brocard et al., 2016a).

### 2.3. Current pattern of precipitation

Moisture tracking from the Pacific Ocean and from the Caribbean Sea is intercepted by the slopes that face the western and eastern coasts of Guatemala, as well as the Petén lowlands in the north (Fig. 4). The AC range receives 4-6 $m.yr^{-1}$ of mean annual precipitation along its northern flank in the Zona Reina (Thattai et al., 2003). In the west, the Central American Volcanic Arc intercepts moisture rising from the Pacific Ocean. In the east, moisture from the Caribbean Sea is channeled along the Lake Izabal basin and then rises up the northern flank of the SM range. Fog interception represents a substantial part of the annual precipitation above 2,000 m in the SM range (Holder, 2004). The volcanic arc, the SM range, and the AC range cast rain shadows over the Corridor Seco (Machorro, 2014), and in particular over the SC range, which receives little precipitation. Semi-arid climate is reached on the floor of the valleys that surround the SC range.

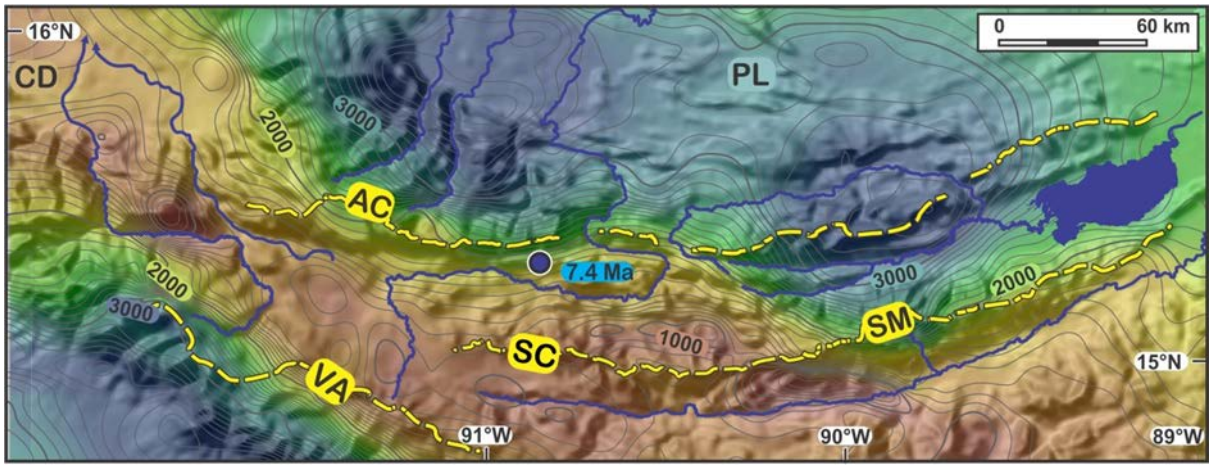


Figure 4. Mean annual precipitation across the study (MARN, 2017) from dry (red) to wet (blue). Isohyet spacing: 100 mm, draped over the shadowed GTOPO 30 DEM. Yellow dashed lines: range drainage divides. Blue dot: location of the fossil forest of Sicaché, buried below a 7.4 My-old ignimbrite (Brocard et al., 2011). CD: Central Depression of Chiapas, AC: Altos de Cuchumatanes, PL: Petén lowlands, SC: Sierra de Chuacús, SM: Sierra de las Minas, VA: volcanic arc.

### 2.4. Bedrock lithology

Rock belts in Central Guatemala tend to follow the strike of mountain ranges (Fig. 5). Late Cretaceous schists and gneisses of the Chuacús Fm. form the core of the SC-SM range. They are flanked by the late Cretaceous migmatites of the San Agustin Fm., and by the marbles and amphibolites of the Jones Fm. In the north, this metamorphic core is tectonically juxtaposed across the Baja Verapaz shear zone to the basement of North America, which mostly covered by a Permian megasequence of terrigenous sediments and carbonates (Sacapulas, Tactic-Esperanza, and Chochal Fms.(Anderson et al., 1973)). These units are intruded by Ordovician (e.g. Rabinal), Triassic, and Jurassic (e.g. Matanzas) granites.

A megasequence of continental terrigenous sediments (the Todos Santos Fm.), Cretaceous carbonates, and Cretaceous evaporites (Cobán Fm., Campur Fm.) covers much of the AC range (Fig. 5). Ultramafic rocks obducted over the carbonates in Late Cretaceous (Campanian) time are preserved within weakly metamorphic synformal klippes (Baja Verapaz, Santa Cruz, and Juan de Paz ophiolites). Higher grade serpentine mélanges crop out along the Motagua valley (Flores et al., 2013).

The southern base of the SC-SM range is incised into sediments deposited in elongate transtensional basins that formed along the Motagua fault (Ratschbacher et al., 2009). During Eocene times (Newcomb, 1975) one such basin was filled by the red beds of the Subinal Formation (Fig.5), which has an exposed thickness of ≥1,500 m (Hirschman, 1962). Its

sediments were provided by the current basement of the SC-SM range, and by the more mature fluvial sediments of an axial river that prefigures the current Motagua River (Guttiérrez, 2008). It now lies in tectonic contact against the SC-SM basement rocks, usually along high-angle reverse faults (Muller, 1979; Bosc, 1971a).

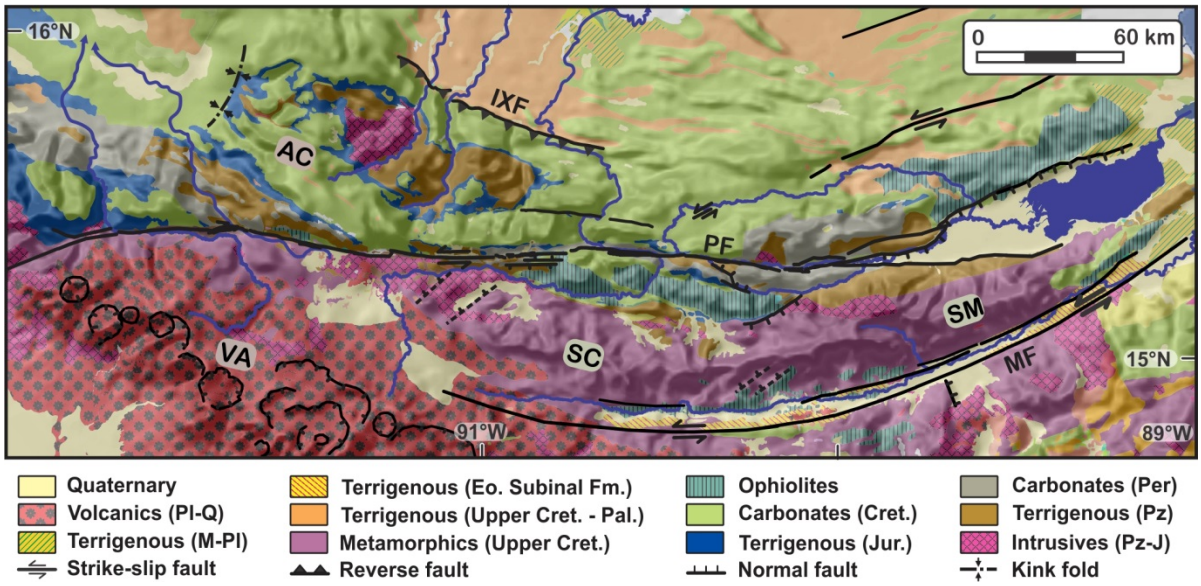


Figure 5. Geology and structure of Central Guatemala (Instituto Geográfico Nacional de Guatemala; Instituto Hondureño de Geología y Minas; Instituto Nacional de estadística y geografía de México), draped over the GTOPO 30 DEM. AC: Altos de Cuchumatanes, IXF: Ixcán fault, MF: Motagua fault, PF: Polochic fault, SC: Sierra de Chuacús, SM: Sierra de las Minas, VA: volcanic arc.

## 3. Methods

### 3.1. $^{40}$Ar-$^{39}$Ar radiometric dating of volcanic rocks

The age of the low-relief Maya surface has been constrained previously using bracketing age markers (Brocard et al., 2011). To improve the dating of the Maya surface we dated andesite boulders embedded in a lahar deposit that rests on the Maya surface, at the western termination of the SC-range near the locality of Chujuyúb (Fig. 2). To establish the chronology of incision of the Motagua valley, we used previously dated alkaline basalts located on the floor of the Motagua valley (Tobisch, 1986), and dated a basalt flow located 500 m above the Motagua River in the foothills of the Sierra de las Minas, near the town of El Jute (Bosc, 1971b) (Fig. 6). Two $^{40}$Ar/$^{39}$Ar whole-rock ages were retrieved from the basalt of El Jute, and

one whole-rock age was obtained on the basaltic andesite of Chujuyúb by the U.S. Geological Survey (USGS) in Denver, CO, USA (see Supplement 1).

### 3.2. Terrestrial $^{10}$Be erosion rates

We measured the concentration of $^{10}$Be in quartz grains extracted from soils and river sediments. We used their $^{10}$Be concentration to calculate hillslope erosion rates, integrated over the past $10^3$-$10^4$ years (see Supplement 2). The soil and rock samples were collected along ridgelines in the SM range. They provide erosion rates restricted to the site of sampling (Table S2-1, Fig. S2-3c). Three of these samples consist of quartzose vein fragments exhumed from weathered orthogneiss, while the two remaining samples come from a highly weathered pegmatite that crops out on the monadnock of Cerro las Palomas, in the Montaña El Imposible (Fig. S2-3b).

The majority of the samples, however, consist of riverborne quartz collected in the bed of 30 rivers in the SM, SC, and AC ranges (Fig. 6, Table S2-2, Fig. S2-3). They provide catchment-averaged hillslope erosion rates (Brown et al., 1995). The quartz was extracted from the sand grain-size fraction (250-500 µm) of the river sediments. $^{10}$Be production increases rapidly with elevation. As a result, systematic altitudinal variations in the concentration of quartz of the source rocks may distort the calculation of erosion rates. Such layout in encountered in AC range (Fig. S2-3a), in which a sensitivity analysis to this effect was conducted. The $^{10}$Be production was weighted according to estimates of the quartz concentration in the source rocks. Weathering is intense in tropical mountains, promoting the concentration of quartz in the soils, and an underestimation of erosion rates that increases with increasing weathering intensity. An assessment of the effect of quartz enrichment was therefore conducted (Table S2-2), using quartz enrichment values from mountain tropical soils of Puerto Rico (Ferrier et al., 2010). The sampling was further designed ~~such as~~ to document erosion rates within nested catchments (Fig. 6. Fig. S2-3a,b), in order to capture along-stream variations in erosion rates, such as those produced by headward-migrating knickpoints (Willenbring et al., 2013b; Brocard et al., 2015b). The samples were prepared at the $^{10}$Be extraction laboratory of the Department of Geology and Geophysics at the University of Minnesota, as well as at the PennCIL lab of the Earth and Environmental Sciences department at the University of Pennsylvania (see Supplement 2).

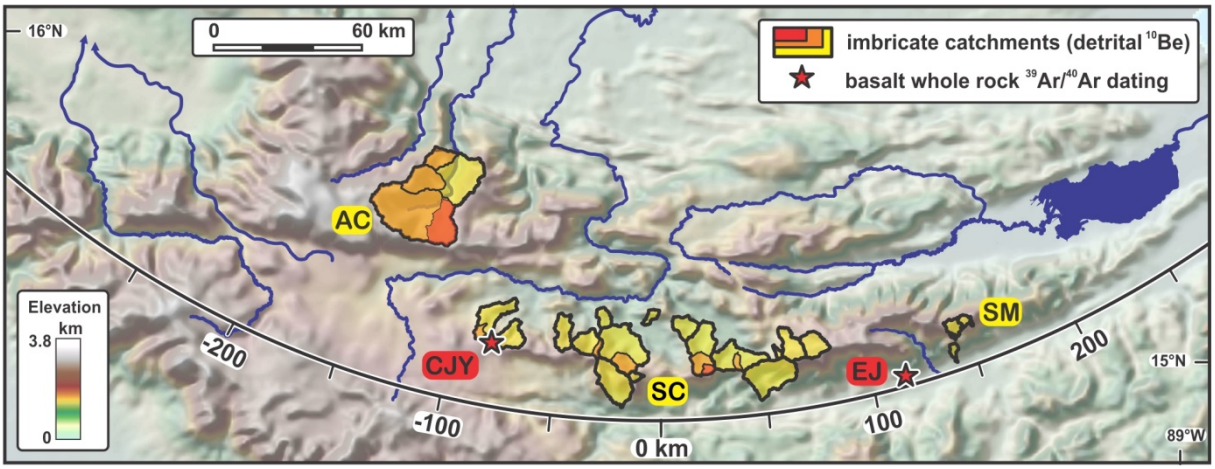


Figure 6. Catchments sampled for the $^{10}$Be analysis (AC: Altos de Cuchumatanes, SC: Sierra de Chuacús, SM: Sierra de las Minas), and $^{40}$Ar/$^{39}$Ar dating (CJY: Chujuyúb, EJ: El Jute). Enlarged maps of the catchments and their lithologies are provided in Fig. S2-1). The arcuate line represents the axis used for plate boundary-parallel projections of Figs. 10 and 12.

### 3.3. Calculation of an erosion index

To test the influence of hillslope steepness and precipitation on $^{10}$Be-derived erosion rates, we calculated a normalized erosion index (Montgomery and Stolar, 2006; Finnegan et al., 2008) over the study area, and averaged it over the extent of the sampled catchments. In its simplest form, the erosion index (EI) correlates the entrainment of particles to hillslope steepness and annual rainfall. We used a formulation in which this entrainment is assumed to be proportional to shear stress: Eq. (1):

$$EI = Q^{1/3} \cdot S^{2/3} \quad (1)$$

where Q is discharge (in $m^3 \cdot s^{-1}$) and S the along-slope gradient ($m \cdot m^{-1}$). Slope was extracted from the national Guatemalan IGN DEM at a resolution of 20 m, and discharge was calculated using mean annual precipitations provided in the MARN (2017) report. Rainfall values were corrected for evapotranspiration, using a map of vegetation from the MARN (2017) report, and evapotranspiration values from the Puerto Rico GAP project (Gould et al., 2008), which amount to 10-82% of the total rainfall, for the different types of vegetation reported in the MARN report. EI values were normalized to the highest obtained EI value within the study area.

### 3.4. River profile segmentation

We extracted the long-profiles of 220 rivers located in the AC, SC, and SM ranges, using the Guatemala national 20 m-resolution DEM released by the National Geographic Institute of Guatemala. The beds of these rivers were observed on stereoscopic couples of aerial photographs provided by the National Geographic Institute of Guatemala (see next section for details). These observations allowed us to sieve out rivers along the expression of longer-term river dynamics is hidden by shorter-term adjustments to karstic disturbances, debris flows, and deep-seated landslides. A subset of the 110 rivers that best capture long-term trends was used in the final analysis (Fig.7).

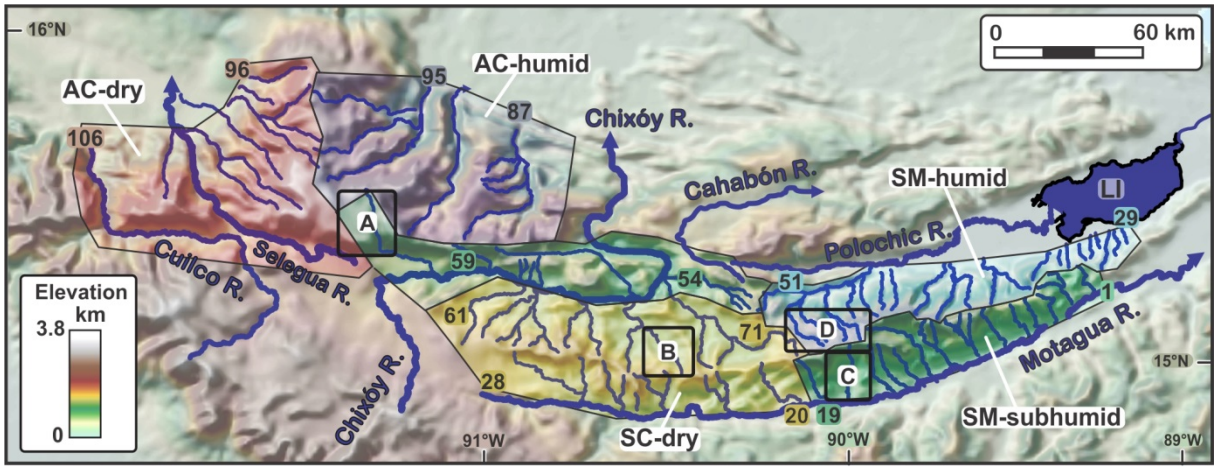


Figure 7. Distribution and grouping of the streams used in the river long-profile analysis, and their grouping by geographic areas. AC: Altos de Cuchumatanes, LI: Lake Izabal, PF: Polochic fault, SC: Sierra de Chuacús, SM: Sierra de las Minas. Numbers (1-106) correspond to the numbers ascribed to the rivers, as listed in table S4-1. The corresponding river profiles are presented on Figs S4-2 to S4-7, and on Fig. 12. Boxes A-D: footprints of the maps displayed on Fig. 8.

To identify knickpoints along the river profiles, we resort to a linearization method that filters out the downstream increase in stream discharge. We chose the integral method (Perron and Royden, 2013), in which elevation is plotted (on chi-plots or χ-plots) as a function of chi (or χ), which is an upstream integral of incremental upstream distance, divided by a normalized local drainage area: Eq. (2):

$$\chi = \int_{xo}^{x} \frac{Ao}{A(x')}^{\frac{m}{n}} dx' \qquad (2)$$

where $A$ and $x$ are the drainage area (in $m^2$) and upstream distance (in m), respectively; $Ao$ (in $m^2$) a reference drainage area and $xo$ a reference upstream distance taken at the same point, $m$ and $n$ two exponents that encapsulate the influence of drainage area and of local slope on river incision rate, respectively. This method overcomes ~~a lot~~ of the scatter that plague earlier linearization methods(Whipple and Tucker, 2002; Goldrick and Bishop, 1995). One of its caveats, however, is that it requires a foreknowledge of the intrinsic concavity, or θ, defined as m/n. The value of θ can be determined by incrementally fitting river profiles to a straight line (Mudd et al., 2014). Such approach is convenient on river profiles made up of a small number of successive segments. Many rivers in the study area, however, have highly segmented profiles (see section 4.3), preventing convergence toward a single value. Besides, the value of θ may change along-stream as a result of changes in climate (Murphy et al., 2016) or changes in the dominant erosive processes operating on the streambed (Brocard and Van der Beek, 2006) such as the alternation of detachment-limited (Howard, 1994) and transport-limited river incision (Whipple and Tucker, 2002), or such as the alternation of sediment-starved and overfed reaches (Sklar and Dietrich, 2006). Therefore, instead of fitting θ to each river profile, we applied a common normalizing concavity $\theta_n$ value of 0.5 to all river profiles, after assessing best fit values on a subset of streams (see Supplement 3). This initial screening showed that most concavity values range between 0.4 and 0.6, as predicted by theoretical studies (Perron and Royden, 2013; Whipple, 2004), supporting the choice of a concavity of 0.5.

### 3.5. Classification of stream segments

The morphology of the streambeds was examined along each linearized segment using stereoscopic black-and-white 0.5-m resolution aerial photographs taken in 2001 provided by the Guatemala National Institute of Geography (see Supplement 4). Observations were punctually ground-proofed during field work campaigns stretching over 6 years. River beds were grouped into types according to the bed component that dominantly determines river gradient along each segment, namely: bedrock, bedrock and gravel bars, gravel bars over bedrock strath, gravel bars over thick alluvial fill, colluvium, large immobile boulders, boulders and gravel bars, boulders and bedrock (Table S4-1). Classification failed in many headwater channels because their bed is masked by overhanging riparian vegetation. The classification roughly reflects differences in the factors that determine stream incision. River incision is indeed likely detachment-limited along bedload-dominated reaches, and transport-limited along gravel- and cobble-dominated reaches, lying over bedrock straths (Tucker and Whipple, 2002; Brocard and Van der Beek, 2006). Boulder-armoured reaches are chocked by slowly- to non-moving boulders that act more like bedrock than bedload, and are therefore detachment-limited. However, unlike other types of bedrock channels, these boulder channels do not reflect the erodibility of the underlying bedrock, but that of surrounding hillslopes, because the majority of the boulders originate from the valley sides. Changes in streambed type from one segment to the next assisted the classification of river knickpoints (see following section).

### 3.6. Classification of river knickpoints

Convex-up breaks-in slope along river profiles are commonly referred to as river knickpoints. For convenience, we refer here to all breaks-in-slope, whether convex or concave, as knickpoints. Knickpoints were classified as lithogenic, alluvial, tectonic, migrating and miscellaneous (see supplement 4). Miscellaneous knickpoints represent adaptations or river profiles to local, stochastic disturbances (such as landslides and epigenies), and are usually short-lived. Most knickpoints in the study area are adaptations of river gradients to along-stream variations in rock uplift rate, bedrock erodibility, sediment flux, or sediment grain size. These knickpoints can be regarded as steady, inasmuch as their location only changes very slowly along the river profiles, tracking spatial changes in the distribution of rock types, rock uplift, sediment fluxes and bedload grain size. By contrast, knickpoints that spearhead step-increases or step-decreases in river incision rates migrate in the upstream direction along river profiles in the form of waves of accelerated (Rosenbloom and Anderson, 1994; Merritts et al., 1994) or decelerated incision (Howard, 1997). They are hereafter referred to as migrating knickpoints, for they usually migrate faster than the knickpoints previously described. Concave-up migrating knickpoints commonly mark the transition from detachment-limited to transport-limited river incision (Whipple and Tucker, 2002) are usually found at the apex of alluvial fans (Fig. 8c), and pediments (Fig. 8b).

Theoretical geometric differences between migrating and steady knickpoints in linearized spaces have been used to discriminate unstable, migrating knickpoints from stable, equilibrium knickpoints (Goldrick and Bishop, 1995; Perron and Royden, 2013; Whipple and Tucker, 2002). In $\chi$-space, upstream migrating knickpoints which celerity is controlled by the stream power law, and that propagate along various branches of a single drainage through a homogenous substrate affected by homogeneous rock uplift, should all share the same elevation and the same $\chi$ value (Royden and Taylor Perron, 2013). In the real world, however, variations in bedrock erodibility, climate, and rock uplift often scatter these values, challenging interpretations based on these sole geometric properties, in particular in areas where environmental heterogeneities generate steady knickpoints which heights and wavelengths are similar to that of migrating knickpoints interspersed among them.

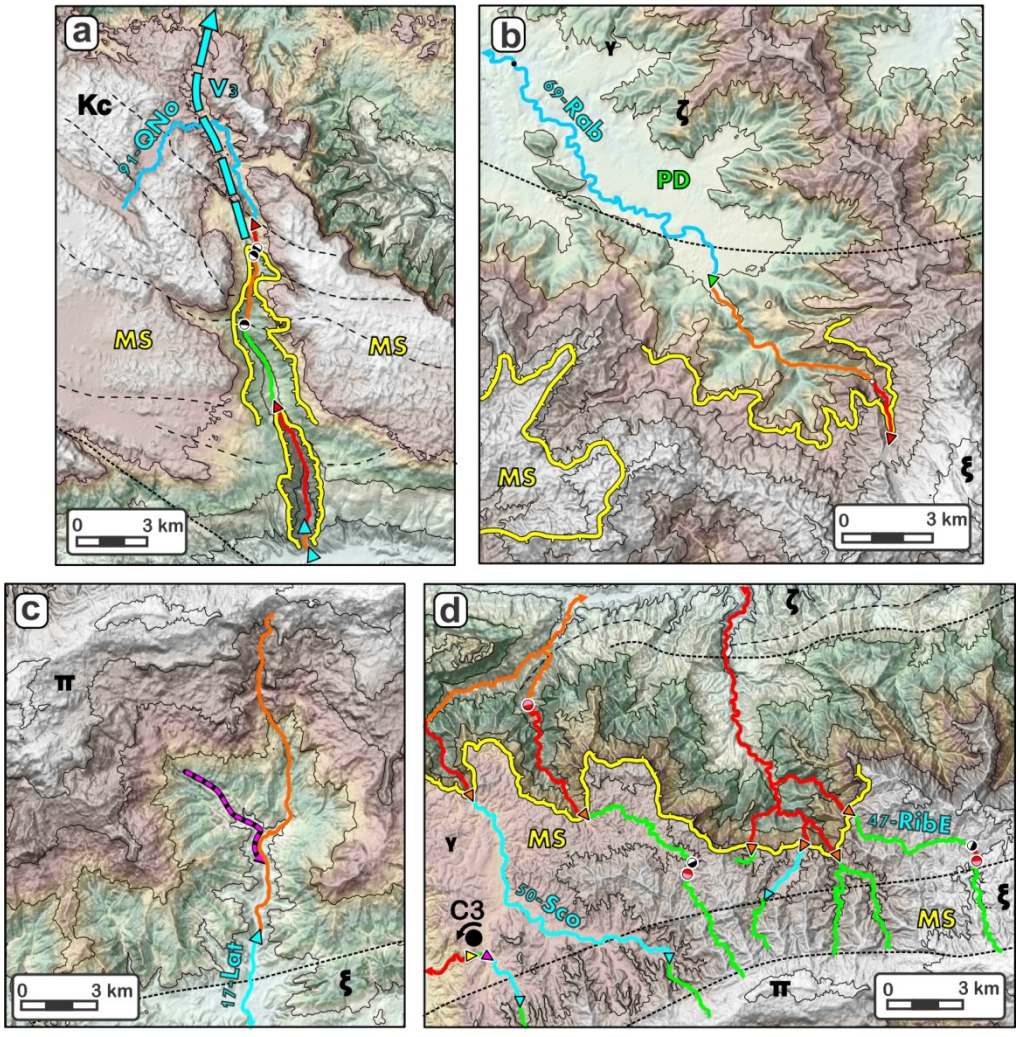
a
Kc
V3
91-QNo
MS
MS
0
3 km
b
69-Rab
PD
MS
0
3 km
c
0
3 km
17-Lor
d
MS
47-RibE
50-SCo
C3
MS
0
3 km
Knickpoint types:
migrating
migrating in soft subtrate
lithogenic
pediment apex
structural
alluvial fan apex
Nature of stream bed:
bedrock
boulder
gravel-covered strath
gravel fill
debris flow
Landforms:
front of erosion
paleovalley # V3
Bedrock structure:
lithological unit boundary
bedding/cleavage trace
Other:
capture site
MS Maya surface
Lithology:
Kc Cretaceous limestone
serpentinite
phyllite
gneiss
granite

340

Figure 8. Examples of some knickpoint types in their geomorphic setting. Shaded and sloped 20 m resolution ALOS DEM © JAXA. Location of maps on Fig. 7. (a) valley of the Quilén Novillo-Chancol river (91-QNo, AC Range), showing paleovalley V3 (fig.2) shallowly incised into the Maya surface (Brocard et al., 2011), and two imbricated waves of erosion migrating up the reversed (southward-directed) drainage of the valley. (b) typical stepped topography of the SC range, in the valley of the Rabinal river (69-Rab), showing three, imbricate, upstream-migrating erosive signals distributed along the mountain slope. The upper one is a wave of erosion that dissects the Maya surface, half-way down the mountain flank one finds a second wave of increased erosion, while the basal and final wave is composed of pediment (PD) apexs that spearhead the upstream growth of pediments. (c) Diffusive erosion in serpentinite mélanges, in the catchment of Río Hato (17-Lat, SM Range). (d) dissection of the Maya surface by prominent migrating knickpoints along the northern flank of the SM Range, from the Ribaco to the Chilasco Rivers (47-Rib to 50Sco). C3: 200 ky-old avulsion site (Brocard et al., 2012).

Under such circumstances, additional discriminating elements must be used. As a first screening, we checked whether the observed knickpoints coincide with marked variations in bedrock erodibility, rock uplift rates, or local anomalies, in which case they were regarded as steady. To assess the effect of lithological variations we used the 1:50,000 and 1:250,000 geological quadrangles of Guatemala, and topical geologic maps from published papers (e.g. (Brocard et al., 2011; Bosc, 1971a). The stereoscopic black-and white 0.5-m aerial photographs of the Guatemala National Institute of Geography were used to refine the location of lithological contacts, and to assess the effects of bedrock fabric, fault damage zones, active faults, deep-seated landslides, and large debris flows on the location of the knickpoints. We used our foreknowledge of the active tectonics of the area (Authemayou et al., 2011a; Authemayou et al., 2012; Brocard et al., 2012) and of Quaternary drainage reorganization (Brocard et al., 2012) to assist the identification of tectonic knickpoints and of some migrating knickpoints. The remaining knickpoints were then considered as potentially migrating. We then looked for supporting evidence, such as geomorphic markers of knickpoint migration, in particular break-in-slopes running along valley flanks, tied to specific knickpoints (Fig. 8a,b) after verifying that such break-in-slopes were not the result of lithological variations along the valley sides. Changes in erosion rates along hillslopes produced by the passage of a migrating knickpoint can also be marked by changes in drainage density, which reflect changes in saprolite thickness (Brocard et al., 2015b). In a few cases the passage of migrating knickpoints was marked by abandoned river terraces and hanging pediments.

The method above has some limitations: first, local variations in bedrock erodibility maybe not be systematically detected, as a result of the imprecision of geologic mapping, especially in the least accessible parts of the SM and AC ranges. Second, large intraformational changes in facies can generate variations in bedrock resistance as sharp as, or even sharper than erodibility differences between mapped geological units. These two effects may lead to the interpretation of stable knickpoints as migrating knickpoints. Conversely, some migrating knickpoints may be pinned to lithological contacts (Crosby and Whipple, 2006), and filtered out by the analysis. Nonetheless, we consider that, given the large number of analysed knickpoints, the analysis captures the most import aspects of the evolution of the landscape within the study area.

## 4. Results

### 4.1. Rock uplift and stream incision chronology from $^{40}Ar/^{39}Ar$ dating

The Maya surface (Fig. 2,3) likely formed close to sea level, because it can be traced to the coast of the Caribbean Sea (Brocard et al., 2011). It was once covered by extensive fluvial deposits, especially south of the Motagua fault, where these fluvial deposits are preserved below extensive ignimbrites (Williams and McBirney, 1969). The lahar deposit of Chujuyúb rests directly onto a thick saprolite that blankets the Maya surface. Lahar emplacement predates the incision of a 450 m-deep valley. The lahar yielded a plateau age of 12.54 ± 0.04 Ma (Fig. S1-1, Table S1-2). It indicates that incision at this site started after 12 Ma. This is consistent with the previously proposed 12 Ma entrenchment of the Cuilco River valley into the Maya surface (Fig.7), 70 km to the NW of Chujuyúb (Brocard et al., 2011), as well as with a 10.3 Ma ignimbrite emplaced in the shallowly-incised Colotenango valley (Fig.2), 35 km to the NNW of Chujuyúb (Authemayou et al., 2012). It is also consistent with a 7.4 Ma ignimbrite deposited in a 1 km-deep paleovalley, incised into the Maya surface (Fig.2), 10-30 km to the NE of Chujuyúb (Brocard et al., 2011). The depth reached by the late Miocene valleys prior to their abandonment implies that incision proceeded at >140-280 $m \cdot My^{-1}$ from 12 to 7 Ma, assuming that the dissection of the Maya surface started at 12 Ma (a, Fig. 9). Incision rates averaged over the length of the valleys between the SC and AC ranges, range from 145 to 205 $m \cdot My^{-1}$ (b, Fig. 9). Subsequent incision, from the base of the late Miocene valley fills, down to modern valley floors, only amounts to a few tens of meters, at rates of <30 $m \cdot My^{-1}$ (c, Fig. 9).

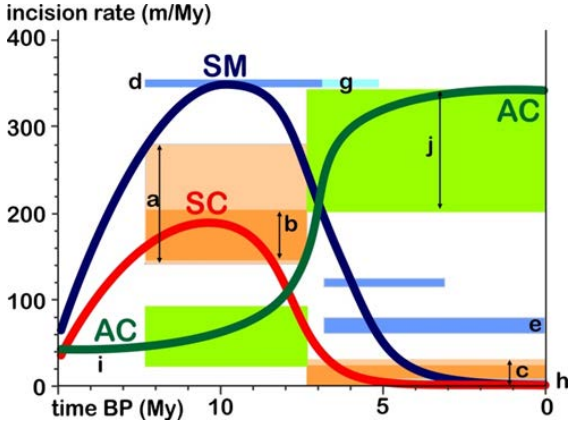


Figure 9. Evolution of incision rates in the studied ranges.

Shades of blue: Sierra de las Minas (SM). Shades of red: Sierra de Chuacús (SC). Shades of green: Altos de Cuchumatanes (AC). a-j: see main text.

The chronology of incision along the southern side of the SC range is documented by remnants of basalt flows scattered along the floor of the Motagua valley. These flows track from vents located south of the valley, in the Caribbean plate (Tobisch, 1986). The outcrop of El Jute represents the distal end of a lava flow which abutted the base of the SM range, backfilling the Huijo River valley with ≥ 70 m of basalt. The base of the flow lies >400 m above the Huijo River. Using the modern gradient of the transport-limited Huijo River as a proxy for its 6 My-old gradient, we find that the basalt flow crossed the Motagua River 360 m above the current elevation of the Motagua River. The basalt yields a plateau age of 6.88 ± 0.03 Ma, and a slightly less constrained total age of 6.46 ± 0.09 Ma (Fig. S1-1, Table S1-2). Assuming that incision of the Maya surface started 12 My ago, then the 2.6 km-deep Motagua valley would have been incised at ~350 $m \cdot My^{-1}$ between 12 and 7 Ma (d, Fig. 9). Incision would have continued until today at an average rate 79 ± 4 $m \cdot My^{-1}$. If the basalt dam was removed rapidly however, then incision would have instead proceeded more slowly, at 59 ± 9 $m \cdot My^{-1}$. The chronology of incision can be refined by incorporating the ages of the previously dated basalts (Tobisch, 1986). The closest occurrence, located 6 km upstream along the Motagua River, is the 6.1 Ma Cerro lo de China flow. The flow was actually emplaced 120 km farther west at current plate-boundary slip rates, because it lies on the southern side of the Motagua fault. Conversely, the 3.1 ± 0.7 Ma Cerro Onanopa was emplaced on the same side of the plate boundary, 16 km upstream of El Jute. Its high vesicularity implies an emplacement at, or near the ground surface, rather than as a sill, deep within the Subinal Fm., followed by exhumation. Its base lies <10 m above the Motagua River. Strath terraces of the Motagua River have been cut in its flanks (Tobisch, 1986), indicating that the flow underwent some minor burial and exhumation. The accordance in elevation between its basal contact and the Motagua River suggests that the Motagua River has oscillated tightly around its current vertical position over the past 3 My. Incision of the Motagua valley, from the elevation of the basalt of El Jute, down to the current valley floor, would thus have occurred between 6.1 and 3.1 Ma, at > 110 ± 40 $m \cdot My^{-1}$ (f, Fig. 9). If, after the emplacement of the basalt of El Jute, incision continued at the same ~350 $m \cdot My^{-1}$ rate as before (g, Fig. 9), then incision would have reached the current valley floor at ~5 Ma, no incision taking place afterwards (h, Fig. 9). The evolution of incision during the rise of the SC-SM range therefore looks similar on either side of the range: it is dominated by a single step of rapid incision, at 140-350 m·My-1, between 12 and 7-5 Ma, followed by an almost complete cessation of incision along the main trunk streams (the Motagua and Chixóy Rivers), which act as base levels of the streams located in the SC range.

Note that large steeply-dipping faults bound the Eocene fill of the Motagua valley. Dip-slip on these faults could be responsible, in part or in whole, for the deepening of the Motagua valley, a possibility contemplated by Tobisch (1986). Various traits of the valley, however, rule out any substantial contribution of these faults. First, fluvial sediments have

bypassed the Motagua valley since Eocene time, feeding a transtensional basin at the lowest eastern d of the Motagua valley. Second, the alluvial fans that have grown astride these faults show no evidence of faulting, nor any anomaly in their catchment/fan surface ratios (Tobisch, 1986). Third, the faults encountered along the base of the SC-SM range exhibit only ancient, ductile to ductile-brittle left-lateral deformation (Bosc, 1971a; Roper, 1978). Last, the middle Miocene low-relief surfaces lie at about the same elevation north and south of the Motagua fault (Simon-Labric et al., 2013). Extension on antithetic boundary faults would need to remain well-balanced, despite hundreds of kilometers of left-lateral displacement along the Motagua fault since the middle Miocene, to avoid the development of significant offsets of these surfaces. The deepening of the Motagua valley therefore appears to have been achieved by erosion, through the removal of the erodible Eocene sediments that filled the Eocene fault basin, giving the valley the appearance of a recently active graben.

The incision chronology of the AC range is constrained by transverse paleovalleys that are shallowly incised into the Maya surface (e.g. Fig. 8a; i, Fig. 9). Uplift of the AC range since their abandonment has allowed the incision of 1,500-2,600 m deep valleys along the northern flank of the range (Fig. 3) at 200-350 $m \cdot My^{-1}$ (j, Fig. 9). River incision of the AC range therefore started and developed while river incision in the SC-SM rang was stalling.

### 4.2. Spatial variations in $^{10}$Be-derived erosion rates

Catchment-averaged detrital $^{10}$Be erosion rates range from 11 $m \cdot My^{-1}$ within the catchments that drain the Maya surface on the SM range, up to 330 $m \cdot My^{-1}$ along the wet and steep northern flank of the AC range (Fig. 10). Most slowly-eroding catchments are located within the SC range. Weighting erosion rates by the relative concentration of quartz in quartz-feeding lithologies marginally affects the calculated rates (by 3.4% on average in the SC range, 4.8% in the SM range, and < 7% in the AC range). Quartz enrichment corrections, on the other hand, increase erosion rates by up to 40% (Fig. 10, Table S2-2), but the amplitude of this effect remains speculative, in the absence of field measurements. However, because quartz enrichment increases with weathering intensity, its effect is probably smaller in the AC range, where soils erode the fastest. Quartz enrichment corrections can be therefore expected to reduce the contrast in erosion rates between the SC-SM range and the AC range.

In the AC range, erosion rates (arrows, Fig. 10) show a marked increase from the drier, and less steep highlands, to the wet and steep frontal slopes (from CATA to CHEL to XAC). The SM range displays a similar trend of increasing erosion down the mountain flank, as entrenchment in the Maya surface increases (from COL to FRI to RAN), with one outlier (SLO). The magnitude of increase is intermediate between that observed in the SC and CA ranges. In the SC range indeed, a downstream increase would be expected initially, in the downstream direction, from the drainage divide down the mountain flanks, from the decreasing contribution of slowly-eroding low-relief uplands with downstream distance (Willenbring et al.,

2013b). It would be followed by a decrease in erosion rates as rivers start draining the pediments that floor the Chixóy River catchment. An increase in erosion rate, downstream of the paleosurface is observed (from PAS to PAE), but it is much less pronounced than in the AC range. The following decrease in erosion rate is also very subdued (from XEU to CUB). In one case (from SMS to SMM to SMI), no increase nor decrease is observed.

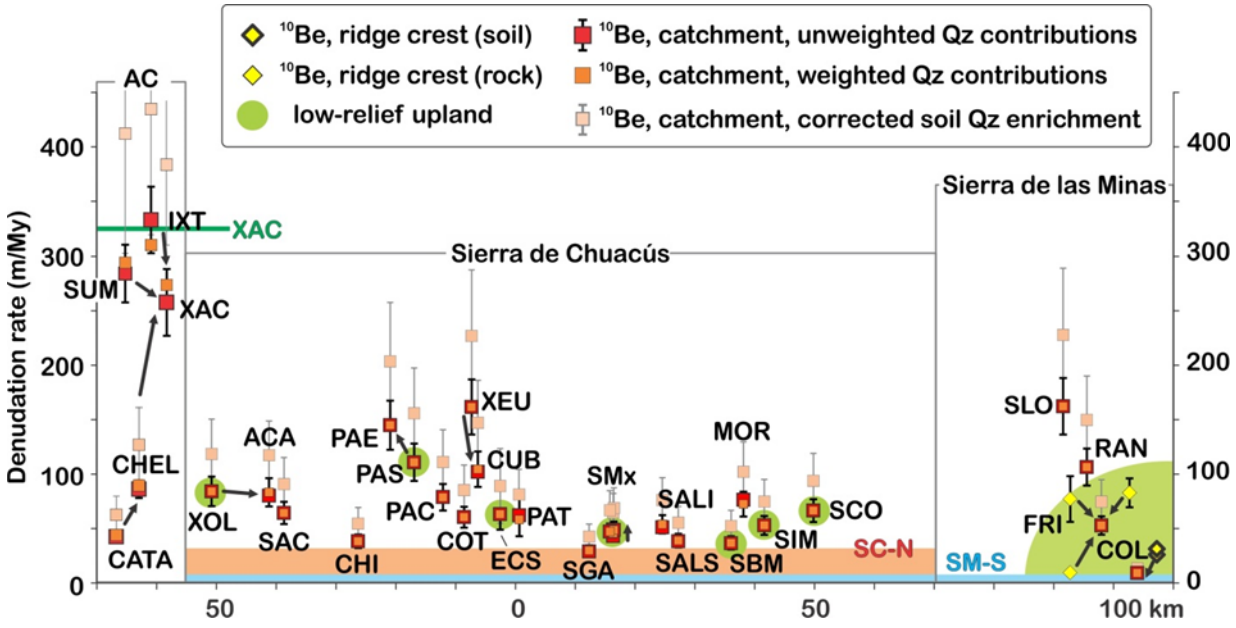


Figure 10. Variations in detrital $^{10}$Be denudation rates along the strike of the plate boundary, from the AC range in the west, to the SM range in the east. Data are projected along the strike of the plate boundary, on an arc displayed on Fig. 6. Arrows shows feeding directions, from hillslope sites to nested catchments. Low relief uplands drain remnants of the Middle Miocene Maya surface. Denudation rates are compared to incision rates along the northern (salmon, SC-N) and southern (blue, SM-S) base of the SC-SM range, over the past 7 My. XAC: peak incision rates in the AC range along Río Xacbal, where incision below the Maya surface along the river course is maximum (Fig. 3).

### 4.3. Distribution of streambed types

9% of the rivers retained in the analysis do not host any knickpoint, 16% host one knickpoint, 51% host 2 to 5 knickpoints, and 25% host 5-12 knickpoints (Fig. 11). This distribution highlights the high degree of segmentation of many rivers in the AC and SC-SM ranges, and the high concentration of knickpoints within these ranges. These knickpoints separate 452 river segments, of which 92% are well linearized, 6% are concave, and 2% are convex, for an applied intrinsic concavity $\theta = 0.5$.

The river segments were grouped by streambed types. Their distribution according to elevation along the studied ranges is displayed on Figure 12, and their distribution between north- and south-facing flanks is displayed on Figures S4-2 to S4-6.

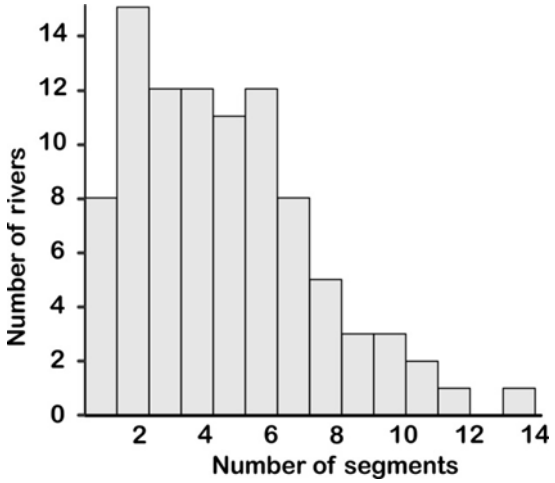


Figure 11. Distribution of rivers according to the number of segments identified in each river

The distribution of alluvial reaches is bimodal in the SC-SM range (Fig. 12a1-b2): alluvial reaches tend to be found either at the base of the mountains, or at high elevation, over the remnants of the Maya surface (e.g. Fig. 8 a,d). High-elevation alluvial reaches tend to transport a rather fine-grained bedload, composed of sand derived from the weathering of micaschist, gneiss and granite, and of gravel derived from quartzose veins and silicified pegmatites (Brocard et al., 2012). Intermediate-elevation alluvial reaches occur upstream of obstructions, most notably landslides in the SM-SC range, over extremely erodible fault damage zones, and within localized areas of tectonic subsidence (especially along the Polochic fault corridor, on the southern flank of the AC range).

Boulder reaches are found mostly on crystalline rocks. They are then more frequent on the wet slopes SM range than on the dry slopes of the SC range. In the SM range, many of these boulder-strewn reaches have formed out of debris flows deposits, by winnowing of their matrix. The SM range is first range hit by Atlantic tropical depressions tracking from the Caribbean Sea. They frequently trigger numerous landslides along its wettest slopes (Ramos Scharrón et al., 2012; Bucknam et al., 2001). Because it soils are more often close to water-saturation, it is also affected by numerous landslides when earthquakes strike the range (Harp et al., 1981). Boulder armoring is also common in the SM range over the serpentinite mélanges that locally crop out up to high elevations along its southern flank, owing to the presence of knockers embedded within the mélanges (e.g. Fig. 8c). Boulder-strewn reaches in the AC range are observed over phyllites. There, the

boulders are made of the most resistant beds of the Pennsylvanian phyllites, and of sandstone and limestone blocks of overlying formations that have sled along the valley flanks.

Bedrock reaches are most commonly found downstream of convex migrating knickpoints, the distribution of which is present in the following section.

### 4.5. Distribution of steady and migrating knickpoints

Among the 350 identified knickpoints, 40% can be tied to variations in bedrock erodibility, 6% to temporary obstructions, 8% to active tectonics, 21% to upstream-migrating waves of accelerated erosion, and 14% to upstream-migrating waves of decelerated incision. 11% are composite and result from some combination of the above.

Details about the significance of the distribution of steady knickpoints is provided in Suppl., as well as a systematic review of the origin of various identified clusters of migrating knickpoints. The origin of some migrating knickpoints can be tied to well-identified and well-dated river Quaternary diversions (e.g. S3-1 to S3-3, Fig. 12a2, (Brocard et al., 2012)). Most migrating knickpoints dot the margins of upland low-relief surface remnants (Fig. 12 a1 and a2; Fig. 8d). They may have therefore initiated farther down their drainage networks, when the Maya surface started being incised, at ~12 Ma on the SM-SC range. Other clusters of migrating knickpoints are found halfway down the flanks of the ranges. The most conspicuous of these is restricted to the northern flank of the SC range, within the watershed of the Chixóy River. It hangs above a series of concave-up migrating knickpoints dotting the apexes of pediments, which extend is also restricted to the drainage of the Chixóy River. The significance of these concave-up knickpoints and their genetic relationship with the cluster of convex knickpoints located above them is discussed in section 5.3.2.

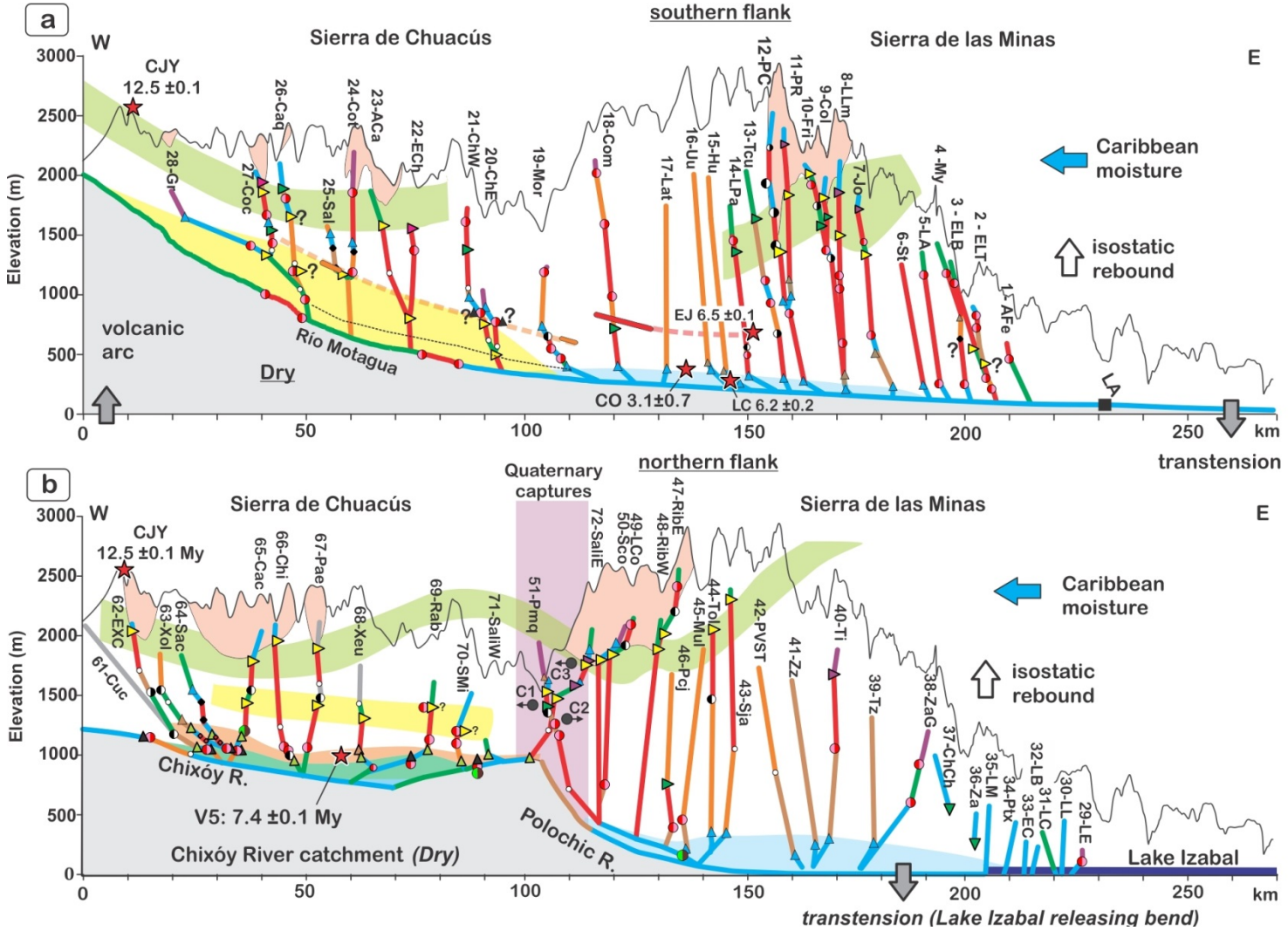


Figure 12. (a) and (b). Distribution of linearized stream segments and knickpoints along the SC-SM range.

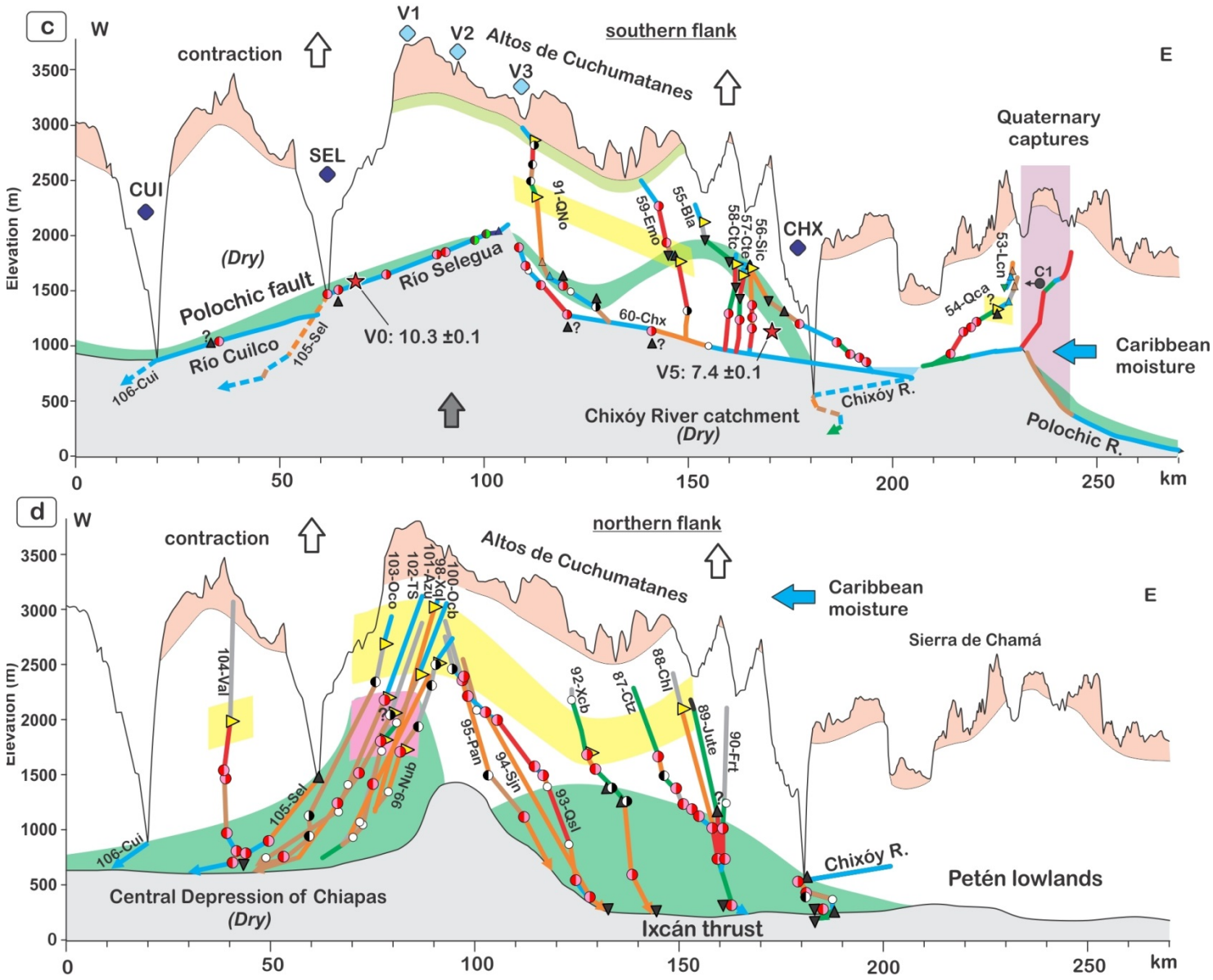


Figure 12.(c) and (d): distribution of linearized stream segments and knickpoints along the AC ranges.

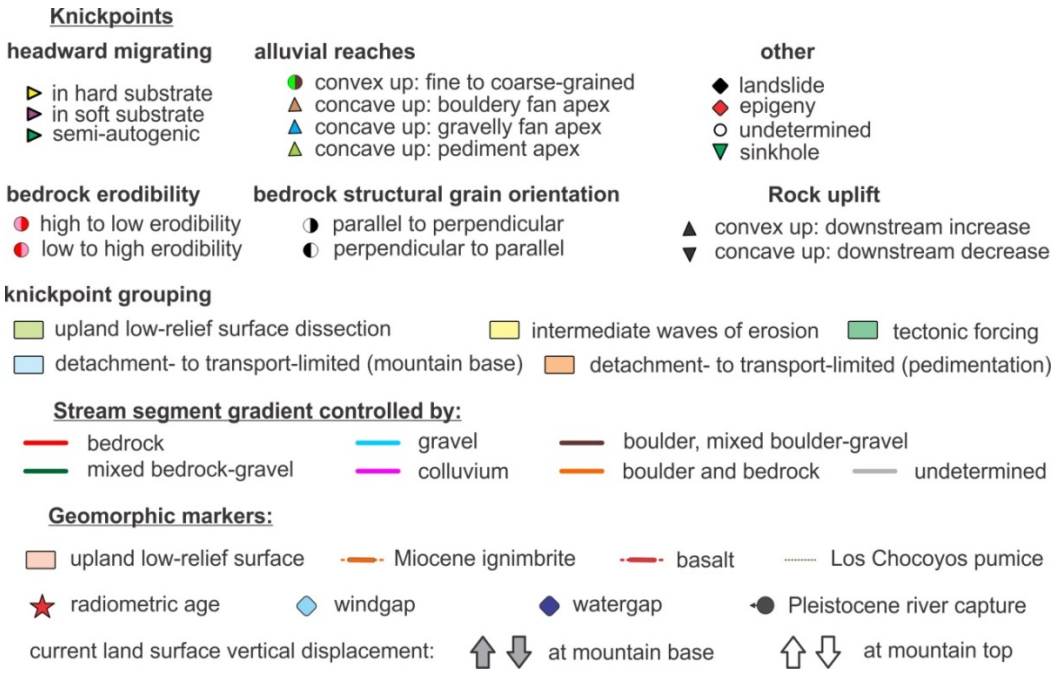


Figure 12. Distribution of linearized stream segments and knickpoints along the SC-SM and AC ranges. Mountain ranges are projected on the plate boundary, according to a small circle defined on Fig. 6. (a) and (b) southern and northern flanks of the SC-SM range, (c) and (d): southern and northern flanks of the AC range. Key to abbreviated stream names is provided in Table S4-1 and in the captions of figures S4-2 to S4-7. Water gap names: CUI: Cuilco, SEL: Selegua, CHX: Chixóy. Paleovalley numbering from Brocard et al. (2011), river capture numbering from Brocard et al. (2012). LA: city of Los Amates.

## 5. Discussion

The decline of river incision rates in the SC-SM range was coeval to the rise of incision rates in the AC range, suggesting that the rise of the AC range was instrumental in the decline of incision rates in the SC-SM range. The AC range may have affected incision rates range in two ways. First, by decreasing moisture delivery to the SC-SM range, it may have

reduced hillslope erosion rates and the delivery of water and sediment to the streams, thereby decreasing river incision rates. Second, by forcing the drainage of the northern side of the SC range to adjust to a new rock uplift field, it promoted a decrease in river incision rates, upstream of the AC, among the rivers of the SC range that still cross the AC range. After reviewing the potential contributions of the top-down and bottom-up processes, we analyse their effects on the present-day morphological evolution of the SC-SM range.

### 5.1. Effect of the rise of the AC range on climate-driven erosion

#### 5.1.1. Climate and hillslope erosion

Silicate weathering has been found to be three times faster on the wet (1,800-3,000 $mm \cdot y^{1}$, Fig.4) side of the SM range than along its drier (1,000-2,400-$mm \cdot y^{-1}$) side (McAdams et al., 2015). Using detrital cosmogenic $^{10}Be$ we find that the the wet (1,900-3,700 $mm \cdot y^{-1}$) side of the the AC range erodes on average distinctively faster (with a 92 % probability, based on a Welch's t-test, with t = 2.246, p = 0.08) than the drier (900-1,300 $mm \cdot y^{-1}$) SC range. Individual catchments document a sixfold increase in erosion (50 to 300 $m \cdot My^{-1}$), from the SC range to the AC range (Fig.10, Fig. 13b,c). The spatial distribution of erosion rates predicted by the Erosion Index (Fig.13a), which combines the effects of slope and precipitation on erosion, is consistent with the spatial distribution of measured detrital $^{10}Be$ erosion rates. $^{10}Be$-source slopes in the AC range receive three times more precipitation (MAP = 3.2 ± 0.7 $m \cdot y^{-1}$) than their counterparts of the SC and SM ranges (MAP= 0.9 ± 0.4 and 1.2± 0.3 $m \cdot y^{-1}$, respectively, Fig.13b ). $^{10}Be$-feeding slopes in the AC range are also 1.2 times steeper (26 ± 4°) than in the SC and SM ranges (22±3 and 22 ± 2°, respectively, Fig.13c). In the AC range, a linear relationship is observed between erosion rate and both precipitation ($r^2$= 0.83) and slope ($r^2$=0.95). This correlation is not as strong when all ranges are considered ($r^2$= 0.61 for precipitation and 0.52 for slope), and very weak within the SC and SM range datasets (-0.1<$r^2$<0.4). The stronger correlation observed in the AC range reflects foremost the greater homogeneity in bedrock erodibility among the measured catchments. Slope gradient and MAP are good predictors of hillslope erosion rates at precipitation is > 2 $m \cdot y^{-1}$ (Fig. 13b), but a linear relationship predicts that erosion ceases for MAP <2 $m \cdot y^{-1}$ and slopes < 15°. It is probable that the curve flattens for MAP < 2 $m \cdot y^{-1}$ a trend observed elsewhere, for example for MAP < 2 $m \cdot y^{-1}$ on Kauai (Ferrier et al., 2013). Low erosion rates (< 50 $m \cdot My^{-1}$) are observed in many catchments of the the SC and SM ranges that still all maintain average slopes ≥ 19 °(Fig.13c), when such low erosion rates are rather observed at slope values < 10° globally (Willenbring et al., 2013a).

For MAP < 2 $m \cdot y^{-1}$, MAP is a poor predictor of erosion rates, likely because storminess and rainfall intensity increasingly become better predictors of hillslope erosion (Liang et al., 2019). The strong correlation between slope and erosion rates in the AC range suggests that slopes have not, on average, reached the critical threshold of slope stability

(Clarke and Burbank, 2010). At low precipitation rates, within the SC range, slope steepness faintly captures some of the variations in erosion rates ($r^2$= 0.41). Comparison between nested individual catchments show that, in 4 out of 6 instances, decreases of increases in EI values are not echoed by significant changes in erosion rates.

It seems therefore that the most arid regions of the study area erode slowly to very slowly, despite maintaining steep slopes, and that slopes, like MAP, become poor predictor of the short-term ($10^3$-$10^4$y) hillslope erosion rates. The pattern of catchment-averaged $^{10}$Be erosion rates points to a role of climate in the erosion of the ranges, in particular in the limitation of erosion on steep slopes. Fluctuations of climate, over millions of years, could therefore affect the long-term evolution of these ranges. This aspect is explored in the following section, in particular the role of mountain building on the climate of Central Guatemala.

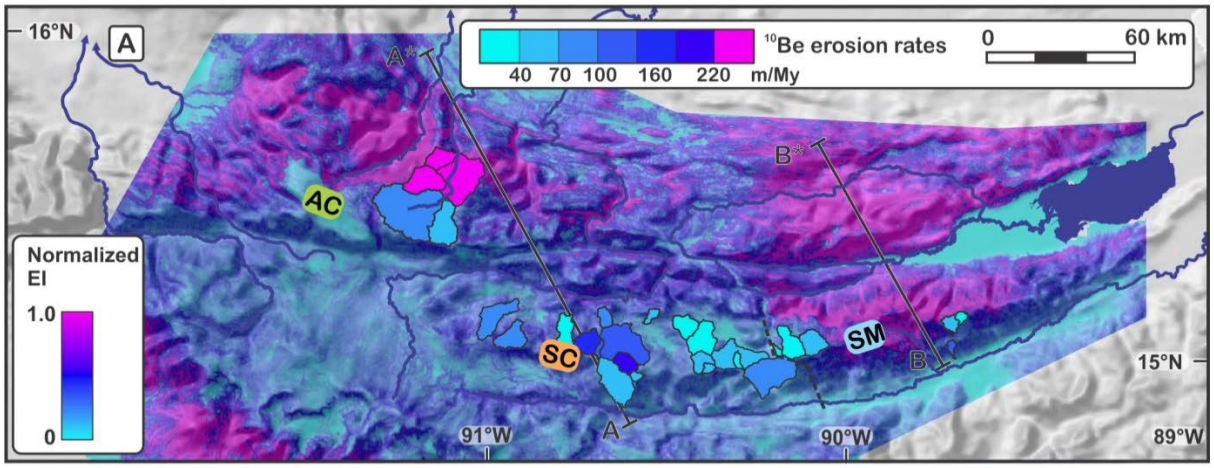

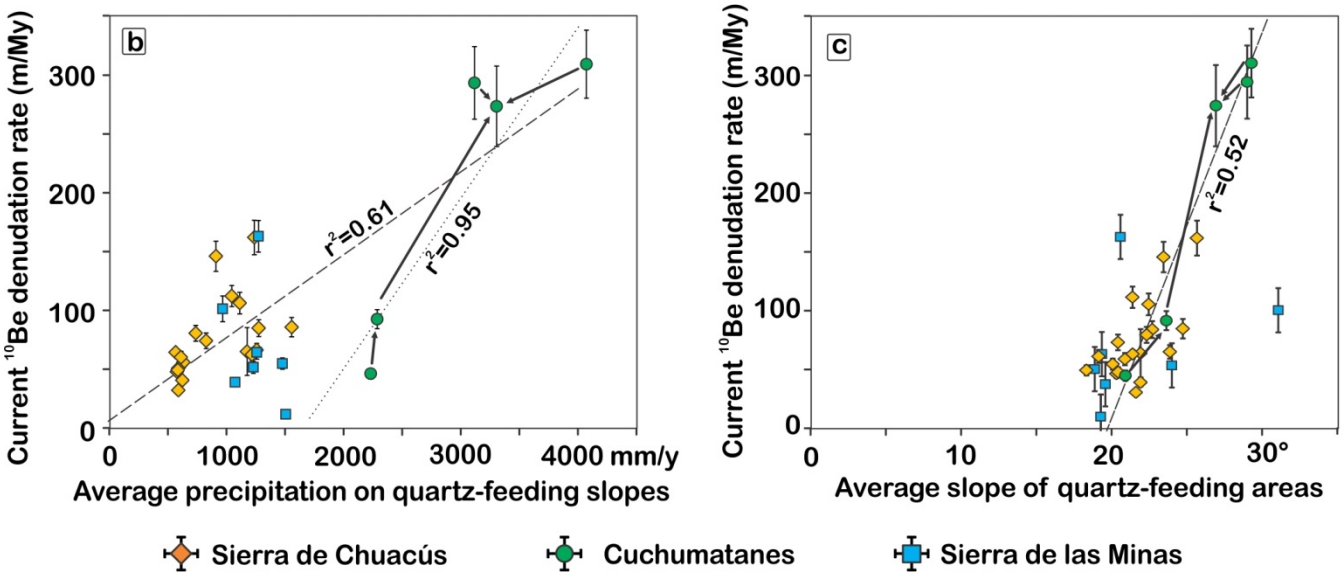


585 Figure 13. (a) Map showing the spatial distribution of normalized catchment-wide $^{10}$Be erosion rates superposed to the predicted spatial distribution of erosion according to the normalized erosion index. (b) catchment-wide $^{10}$Be erosion rates as a function of catchment-averaged precipitation. (c) catchment-wide $^{10}$Be erosion rates as a function of catchment-averaged slope (from quartz-contributing slopes) Arrows: downstream connections between nested catchment within the AC range. Dashed line: linear correlation within AC range data, with correlation coefficient ($r^2$) reported next to the line.

590

### 5.1.2. Evolution of climate driven by the rise of the AC range, and expected consequences on the erosion of the SC range

595 The distribution of precipitation (Fig.2) shows that the AC range currently prevents the ingress of Caribbean moisture tracking from the Yucatán and Petén lowlands. It can be expected, therefore, that moisture was able to reach the SC range before the AC range started to rise. Such a deeper inland penetration of the moisture is confirmed by paleo-precipitation estimates obtained from the study of tree species and paleosols in the 7.4 Ma forest of Sicaché (Fig. 2). The subtropical forest grew on the floor of one of the abandoned late Miocene paleovalleys. The characteristics of the paleosols
600 preserved below the forest suggest mean annual precipitation in the 950-1,300 mm·yr$^{-1}$ range (Brocard et al., 2011). The area where the fossil forest crops out is drier today and covered by xerophytic vegetation. The fossil forest is located on the southern side of the AC range; it documents therefore a deeper penetration of Caribbean moisture toward the SC range at 7

Ma. It therefore suggests that precipitation was higher on the SC range between 12 and 7 Ma, and that it decreased with the rise of the AC range. Drying of the SC range, in turn, can be expected to have contributed to the decrease in hillslope erosion rates over the SC range. Aridification may have changed the balance between water and sediment discharge (Sklar and Dietrich, 2006; Beaumont et al., 1992; Whipple and Tucker, 1999), but if, in the process, streams were left not exceedingly overfed nor underfed with sediment, one can expect river incision to have scaled with stream discharge (Sklar and Dietrich, 2006). In that case the decrease in river incision rates observed at the base of the SC range (see section 4.1) could be, in part, due to the aridification of the SC range. The rise of the AC range could have affected hillslope erosion and river incision over the SC range by such a top-down process, from precipitation to hillslopes to streambeds. However, the AC range also altered the routing of water away from the SC range. In doing so, it sparked a massive adaptation of the drainage to the new tectonic field, to such extend that it also contributed to the decrease in incision rates. This aspect is explored in the following section.

### 5.2. Effect of the rise of the AC range on tectonically-driven river incision

The rise of the AC range results sparked widespread reorganization of the range-transverse drainage (Brocard et al., 2011), leading to the tectonic defeat of many rivers that used to cross the range. The rivers that maintained a course transverse to the rising structure adapted their gradient to the new crustal strain field. We review first the evidence for faster uplift in the AC range than in the SC range, then analyse the consequences of this faster uplift on incision rates long the rivers that cross the AC range, upstream of the AC range, within the SC range. We also analyse the contribution of the rise of the AC range to river course lengthening along the Polochic fault, analyse how this affected river incision in the SC range.

#### 5.2.1. Fast, ongoing rise of the AC range from river channel steepness

The deformation of paleovalleys abandoned during the uplift of the AC range documents >1-2 km of rock uplift in the AC range relative to the SC range since the late Miocene (Brocard et al., 2011). Such deformation implies faster rock uplift rates in the AC range over the past 7 My. Whether such difference remains today is important for analysing river profile dynamics. Glacial and fluvial landforms of the AC range do suggest that that the AC range still rises faster than the SC range. Glacial landforms provide some indirect clues. A 20 x 30 km ice cap spread over the summit plateau of the AC range (Fig. 1) during the last glaciation (Anderson et al., 1973; Lachniet and Vazquez-Selem, 2005). On other neotropical mountains the moraines of the last glaciation are set in older tracts of moraines, left by previous, more extensive ice-caps and glaciers (Lachniet and Vazquez-Selem, 2005). In the AC range, however, they are not observed. Their absence implies that earlier ice caps were smaller than the one that developed during the last glaciation, and that their deposits have been

eroded away by the most recent ice cap. Considering that there is no particular reason why climatic forcing would have affected Central Guatemala in a different manner, the most straightforward explanation is that the part of the range above the equilibrium line of accumulation (ELA), has increased steadily from one glacial cycle to the next as a result of surface uplift, and that this uplift has been significant enough to overcome differences in the intensity between glacial cycles. The effect of surface uplift is made easier by the fact that the top of the range is a plateau, such that small increments of uplift bring large areas of the range above the ELA. The current driver of surface uplift is still contraction (Guzmán-Speziale, 2010; Authemayou et al., 2011b), just as in the early stages of mountain growth, to which erosional unloading may now contribute more than in the early stages, driven by the deep dissection of the northern flank of the AC range.

The steepness of river profiles in the AC range further support the hypothesis that the range still lifts up faster than the SC range. The projection of river profiles in $\chi$ space (Figs. S4-2 to S4-7) shows that, in each of the analysed areas (AC, SC, and SM ranges), linearized segments that share similar streambed conditions (alluvial, boulder-armoured, bedrock) tend form share similar $\theta_n$-normalized steepness (Fig. 14a). Rivers that flow over bedrock are steeper than rivers that flow over immobile boulders, which in turn are steeper than rivers that flow over alternations of gravel bars, or bedrock and boulder, which in turn are steeper than alluvial rivers. Each category, however, exhibit steepness values that change from one range to the next (Fig. 14 b,c,d). It is expected that the bedrock rivers conform to the predictions of the stream power law, because their incision is detachment-limited. At dynamic equilibrium, their steepness should therefore scale with rock uplift, bedrock erodibility and precipitation (Whipple and Tucker, 1999). The progressive increase in steepness from the SC range to the the AC range does not result from an increase in bedrock erodibility, because erodibility is higher in the AC range than in the SC and SM ranges. It does not result either from the observed increase in precipitation from the SC to the AC range, as the increase would instead decrease river gradient. The steeper reaches of the AC range are therefore best explained by faster incision in the AC range, driven by faster rock uplift. This is consistent with the higher $^{10}$Be hillslope erosion rates measured in the AC range, assuming that slopes and channels are well coupled there (Callahan et al., 2019).

Boulder-armoured and alluvial channels are also steeper in the AC range (Fig. 14b,c). Boulders act as bedrock, and boulder-armoured reaches could therefore be expected to evolve like other detachment-limited channels. However, alluvial channels are likely transport-limited, and the slope of transport-limited reaches is less sensitive to rock uplift (Whipple and Tucker, 2002; Cowie et al., 2008). The increase most likely reflects an increase in bedload grain size with increasing erosion rate, resulting from shorter residence times and more limited comminution of bedrock blocks in hillslope soils (Riebe et al., 2015; Neely and DiBiase, 2020).

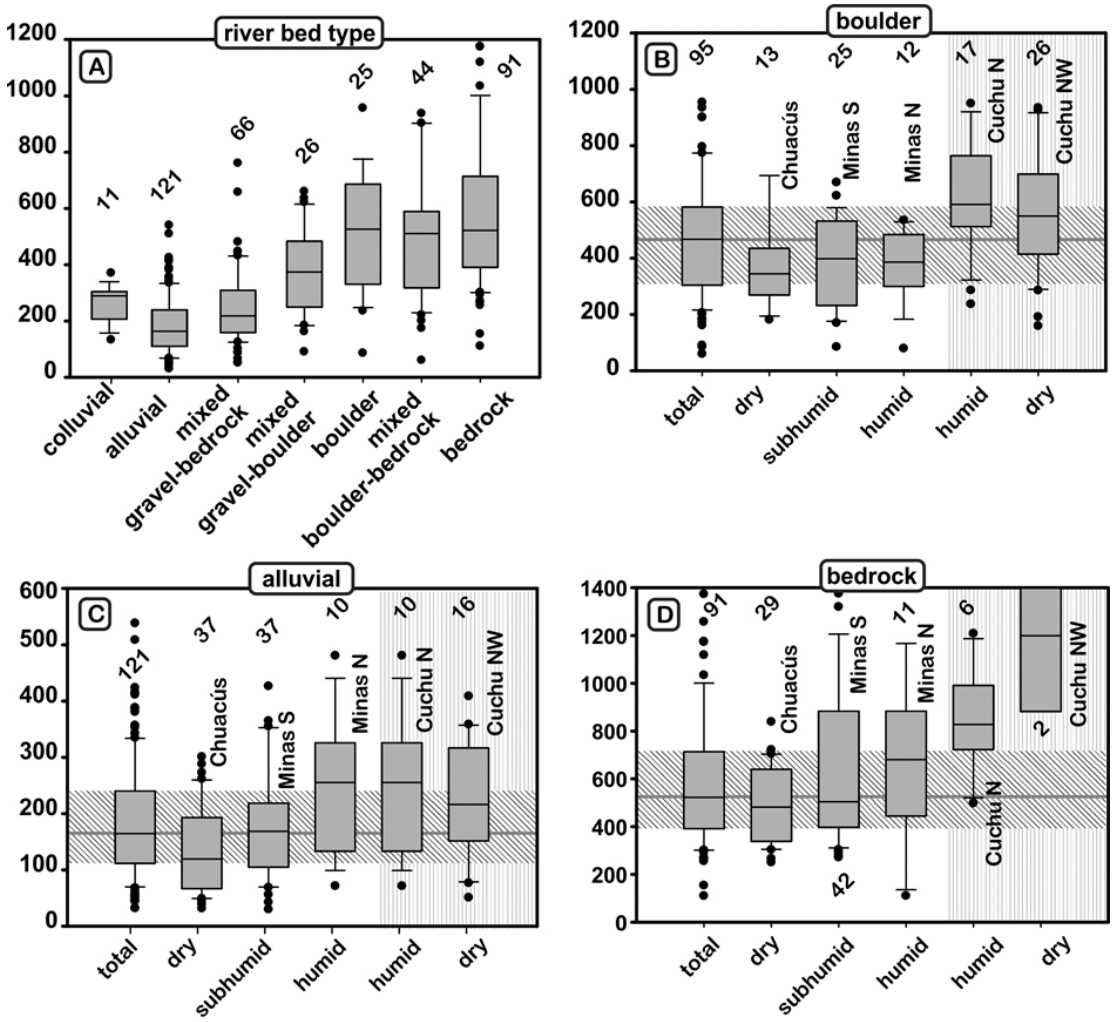


Figure 14. Box plots of stream segment normalized steepness as a function of streambed type and location.
(a) Comparison of steepness by streambed environment; (b), (c), and (c): spatial variations in channel steepness across the study area, according to the regions defined on Fig.7, for the three main types of streambed environment: (b): boulder, (c): alluvial, (d): bedrock. Numbers above box plots: number of segments. Oblique hatches: mean defined by the total number of segments. Vertical hatches: actively uplifting AC range.

### 5.2.2. Tectonic steepening of rivers transverse the AC range

The four rivers that still cross the AC range are the Cuilco, Selegua, Chixóy, and Cahabón Rivers (Fig. 7). The Cahabón River is the smallest these. It is affected by an ongoing pulse of drainage rearrangement that started at ~1 Ma that led to the

shrinking of its headwaters, south of the Polochic fault, a process that will soon lead to its complete beheading south of the fault (Brocard et al., 2012). To analyse the effect of the AC range on the transverse river we therefore focus on the three other rivers. Of these, two exhibit steeper profiles as they cross the AC range, namely the Chixóy and Selegua Rivers (Fig. 15). As they cross the AC range these rivers incise rock formations that they already incise farther upstream, without displaying any similar steepening, from which it can be concluded that the steepening is not caused by the present for more resistant rocks, but instead by faster uplift of the AC range (Leland et al., 1998; Kirby, 2003), consistent with the interpretation of the steepening of shorter rivers draining only the AC range (see previous section). The lack of substantial steepening along the Cuilco River could imply that there, the AC range no longer rises faster than the areas located farther upstream. This interpretation, however, is at odds with documented ongoing contractional deformation nearby (Authemayou et al., 2012). Instead, the lack of steepening may rather stem from the Cuilco River being a transport-limited river over its entire length, as evidenced by its continuous cover of alluvium, in contrast to the Selegua and Chixóy that display an alternation of bedrock and alluvial reaches, typical of detachment-limited rivers. Transport-limited conditions indeed generate less steepening than detachment-limited conditions in response to enhanced rock uplift (Cowie et al., 2008; Whipple and Tucker, 2002). A profuse delivery of volcanic gravel in the headwaters of the Cuilco River, where the river drains the Central American volcanic arc, probably explains this behaviour. The Chixóy River also drains the volcanic arc in its headwaters, but volcanic gravel sources are located farther from the AC range, such that, by the time the Chixóy River reaches the AC range, the petrological composition of its bedload reflect that of the most proximal gravel sources (Deaton and Burkart, 1984), the gravel produced in the arc being comminuted or/and trapped upstream.

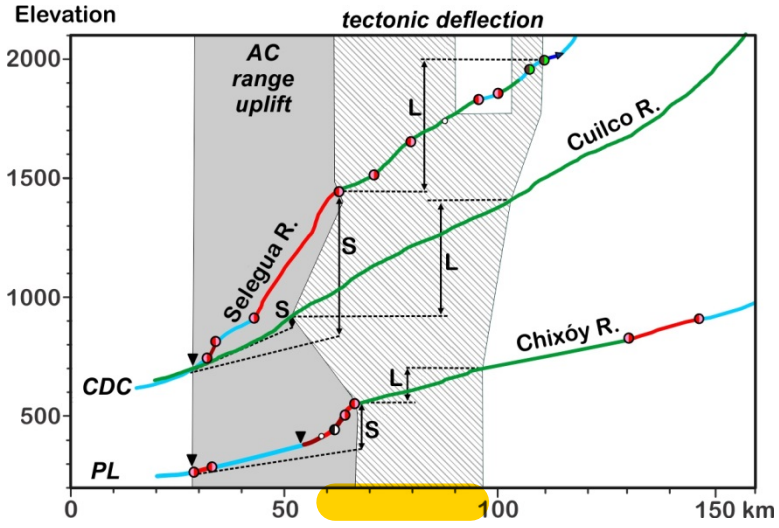

Figure 15. Long profiles of rivers transverse to the AC range: Chixóy, Selegua, and Cuilco, with indications of reaches affected by vertical rock uplift (grey area), and those affected by horizontal lengthening along the Polochic fault (hatched area). S and L: contributions of steepening and lengthening to the uplift of river profiles, upstream of the AC range. River knickpoint nomenclature: see Fig. 12.

### 5.2.3. Transient slowing of incision in the SC range in response to river steepening in the AC range

The steepening of rivers across the AC range represents the response of rivers to the rise of the AC range, in an area previously characterized by a foreland, crossed by shallow-gradient rivers. The phase of steepening, from shallow-gradient rivers to steep-gradient ones, should end with the achievement of an equilibrium state whereby the gradient of the transverse rivers is steep enough for river incision to counterbalance rock uplift in the AC range. For such steepening to occur, the headwaters must rise with respect to the foreland. This results in surface uplift in the SC range. Surface uplift requires a transient imbalance, upstream of the AC range, with incision rates lower than rock uplift rates. The sharp drop in incision rates in the SC range from 145-205 $m \cdot My^{-1}$ to <30 $m \cdot My^{-1}$ after ~7 Ma (see section 4.1) can be viewed, therefore, as driven by the steepening of the Chixóy River in response to the rise of the AC range, because the Chixóy River is the post-7 Ma outlet of most SC range rivers.

Using the river profiles of the Chixóy River (Fig.15), it can be assessed that, ~190 m of surface uplift along the Chixóy can be ascribed to river steepening resulting from the rise of the AC range, at ~27 $m \cdot My^{-1}$. If, before 7 Ma, rock uplift rates in the SC range matched its incision rates of 145-205 $m \cdot My^{-1}$ (Fig.9), then, if such uplift rates were sustained in the SC range after 7 Ma, then 1.5 to 2 My would be necessary to lift up the Chixóy River and its tributaries to their current elevation, upstream of the AC range. Incision would resume afterwards. Such estimates have various limitations, in particular because both the Chixóy and Selegua Rivers experienced large changes in drainage area upstream of the AC range during the 7 Ma reorganization event, which affected their gradient across the AC range (Brocard et al., 2011). The Chixóy River was initially smaller, and therefore probably steeper, before receiving water and sediment contributions from of all surrounding streams at 7 Ma. Conversely, the Río Selegua lost some of its headwaters, and such loss may have contributed to its steepening. The calculation, however, suggest that the timescale of equilibration should be much shorter than the 7 My that have elapsed since the AC range started to rise. Ever increasing rock uplift rate in the AC range would promote continuous steepening, and therefore could prevent the return of incision, upstream of the AC range. Although plausible, such evolution remains speculative, because available data lack the resolution necessary to test it. We identified, however, other processes that delay the resumption of incision along the northern flank of the SC range.

### 5.2.4. Slowing of incision in the SC range in response to river lengthening along the Polochic fault

One such process is the lengthening of rivers as they cross the Polochic fault, before flowing across the AC range. Their course is progressively set off by slip on the Polochic fault, leading to the development left-lateral deflections that lengthen their course. Rivers maintain a gradient sufficiently steep along these deflections such as to allow at least the bypass of their bedload. This results in the uplift of the streambeds, commensurate to the amount of river lengthening. Before the rise of the AC range, such deflections where located in the foothills of SC range, at the entrance of the northern foreland. Streambed uplift, at a place where streambeds are shallowly incised, allowed for repeated avulsions toward the foreland, periodically annealing deflections (Sieh and Jahns, 1984). The rise of the AC range led to deeper entrenchment of tectonic deflections along the Polochic fault, preventing the annealing of deflections, and ensuring that all slip on the Polochic fault results in permanent river lengthening and uplift. The courses of the Chixóy, Selegua, and Chilco Rivers have thus been lengthened by 25-40 km (Fig.7), and the westward increase the length of deflection, in a context of westward decrease of total slip on the Polochic fault (Authemayou et al., 2011b), was interpreted as the result of earlier entrenchment of the rivers in the west (Brocard et al., 2011). River lengthening drove 500, 600 m, and 150 m of surface uplift along the Cuilco, Selegua, and Chixóy Rivers, respectively (Fig.15). Because left-lateral slip rate of the Polochic fault has been fairly steady over the past 7 Ma, at 2.9 ± 0.4 $mm \cdot y^{-1}$ along the tectonic deflection of the Chixóy River (Authemayou et al., 2012; Bartole et al., 2019), river lengthening and uplift, likewise, must have steadily uplifted the upstream parts of the Cuilco, Selegua, and Chixóy River, at 15 ± 2 $m \cdot My^{-1}$ along the Chixóy River. In contrast to river steepening, the effect of such uplift on incision rates, upstream of the AC range, is permanent.

**5.2.5. Respective contributions of tectonics and climate to the stalling of river incision in the SC range**

With estimated rates of ~27 $m \cdot My^{-1}$ and 15 ± 2 $m \cdot My^{-1}$, tectonic steepening and river lengthening are the two bottom-up processes that we could identify that contributed the rise of the AC range, and to some decrease in river incision rates. Still, they only represent a fraction of the drop in river incision rates from 145-205 $m \cdot My^{-1}$ before 7 Ma, to <30 $m \cdot My^{-1}$ after ~7 Ma. Such evolution implies therefore either a substantial decrease in rock uplift rates in the SC range after 7 Ma, or/and a strong effect of the aridification of the SC range on river incision rates.

A decrease in rock uplift rates in the SC range is supported by the difference in elevation between paleovalleys located in the AC range, such as V3 (Fig. 2, Fig.8a), which underwent 2.8 km of uplift since ~7 Ma (assuming an initial foreland elevation of 0.3 km), and the Chixóy River, which only underwent 0.35 km of uplift in the meantime. If the Chixóy River had lifted up since 7 Ma at the rate at which river incision occurred in the SC range before 7 Ma (145-205 $m \cdot My^{-1}$), then the difference in elevation between V3 and the Chixóy River (0.9 km) would be only $1/3^{rd}$ of its present-day value. Their difference in elevation is even slightly smaller than the 1 km back-tilting of paleovalleys V4-V5, south of the Polochic fault (Fig.2 (Brocard et al., 2011)).

Fluvial and volcanoclastic aggradation in the range of 50-300 m occurred along the rivers that drain the northern flank of the SC range prior to 7 Ma, as documented by the sedimentary fills of the paleovalleys, upstream of the AC range. They support the view of a strong imbalance in uplift rates between the two ranges from the start. Such aggradation can be viewed as the transient response of these rivers to increased uplift farther downstream (van der Beek et al., 2002; Attal et al., 2008), due in these case, to the rise of AC range (Brocard et al., 2011). A similar aggradation is observed along the northern drainage in Plio-Quaternary times, along the northern flank of the SM range, in response to the rise of transtensional horsts and tilted blocks (Brocard et al., 2012). The return to pre-aggradation levels would mark the return to equilibrium, characterized by a lack of rock uplift, of the SC range with respect to the foreland, hence the lack of river incision. In this view, the few 10s of meter of incision since 7 Ma would represent a fine balance between river incision and rock uplift in the SC range, with rock uplift providing quite precisely the 350 m of surface uplift needed to counterbalance river steepening in the AC range and river lengthening above the Polochic fault. There is, however, no obvious process whereby such fine balance of rock uplift rates would be achieved.

Alternately, instead of an equilibrium response, the absence of incision could be viewed as an absence of response to tectonic processes, in a landscape subjected to aridification after 7 Ma. By decreasing water discharge, aridification would reduce stream power. This would initially reduce incision in the SC range, while promoting river steepening in both the SC and AC ranges (along rivers which mostly drain the AC range), furthering surface uplift. Second, it may have altered the balance between water and sediment discharge in such a way as to reduce sediment transport capacity and river incision (Beaumont et al., 1992), or limited the availability of tools for eroding the bedrock (Sklar and Dietrich, 2006). A contribution of climate to the slowing of incision is also suggested by the evolution of the southern flank of the SC and SM ranges, which, although exposed to a different tectonic forcing than the northern side of the SC range, underwent a similar evolution of incision rates as the northern flank of the range. There, the only possible contribution of the Motagua River to the stalling of incision would be through a considerable lengthening of its course at its downstream end, into the Caribbean Sea, requiring surface uplift farther upstream in order to maintain the downstream dispersal of sediments. Some lengthening probably occurred as a result of the emergence, at the its downstream end, of a transtensional basin filled with terrigenous sediments that marine middle Miocene sediments (Carballo-Hernandez et al., 1988). This lengthening of >180 km currently involves <75 m of surface uplift. A stalling of incision along the southern flank of the range, would, at equilibrium, involve southward tilting of the range, such as to accommodate the difference in surface uplift. It seems highly unlikely that independent tectonic phenomena, such as the uplift of the AC range in the north, the lengthening of rivers on the Polochic fault, the decrease in rock uplift rates, and the lengthening of the Motagua River in the west, would converge such as to produce the similar stalling of incision on either side of the SC range. The aridification of the range, which is well documented on either side (Machorro, 2014), appears therefore as an import factor, slowing down river incision.

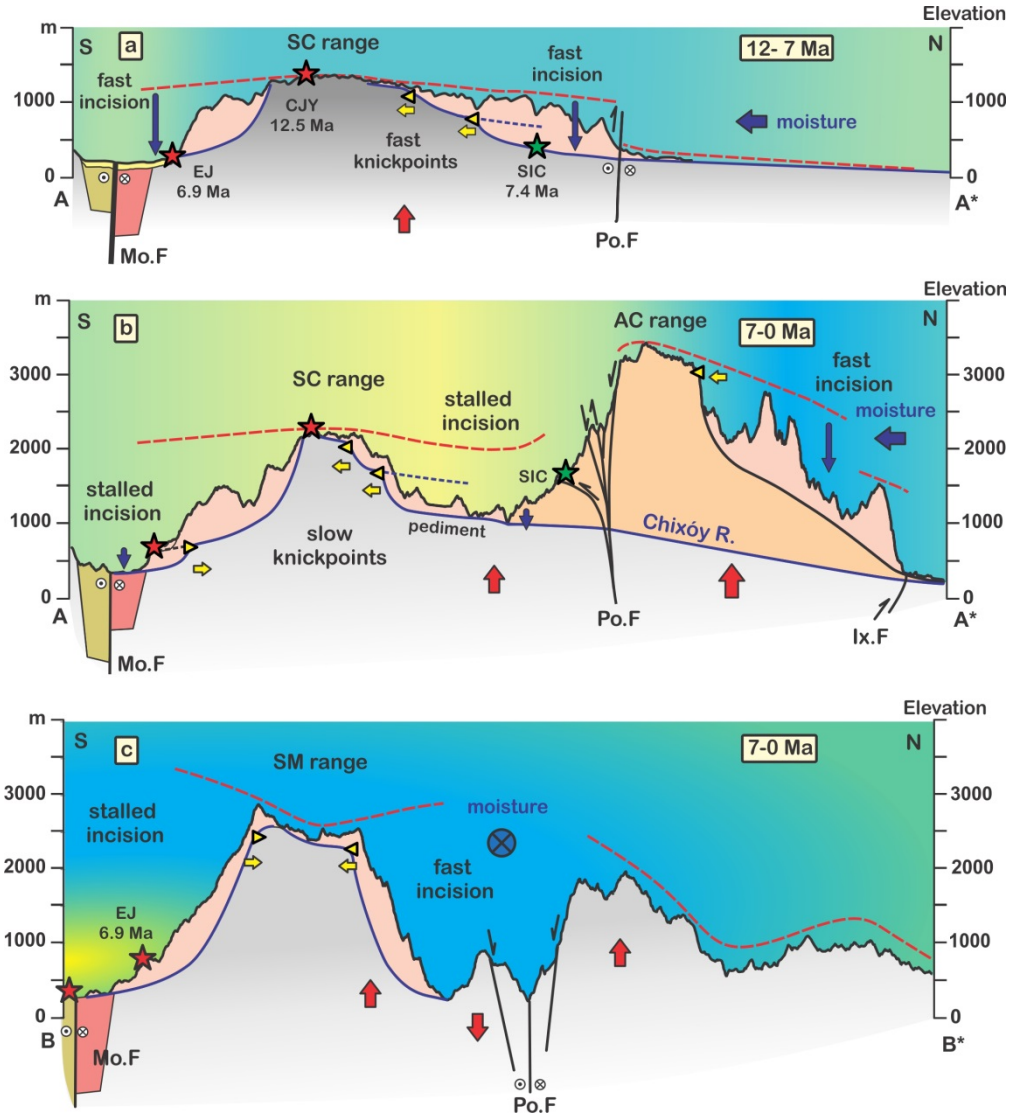


Figure 16. Development of the central ranges of Guatemala. Along profiles A-A* and B-B* (see Fig. 13a for location).

### 5.3. Topographic evolution of the SC range in response to the uplift of the AC range

795

#### 5.3.1. Slowing down of hillslope erosion, topographic decay, and backwearing

Modern $^{10}$Be-derived hillslope erosion rates SC are higher (> 50 m·My$^{-1}$) than the <30 m·My$^{-1}$ long-term river incision rates around the SC range (Fig.10). This suggest that the relief of the SC range has been slowing decaying over the

past 7 My. Hillslope degradation during decay could possibly account the lower average steepness of quartz-feeding slopes in the SC range (22±3°) compared the AC range (26 ± 4°). Hillslope steepness degradation should be associated with a decrease in the local relief of the SC range. The preservation of the Maya surface on many summits, combined with the absence of substantial incision around the base of the range however imply that the height of the SC range has not been been significantly reduced over the past 7 My. Instead, decay appears to have proceeded through the backwearing of the slopes, from the base of the range towards its divide. This is manifested by the development of pediments that expand towards the range interior, and by the presence of upstream-migrating river knickpoints within these backwearing slopes.

### 5.3.2. Origin of migrating river knickpoints within the SC range

Three clusters of migrating knickpoints are found at different elevations along the northern flank of the SC range (Fig. 8b and 12a2). The uppermost cluster consists of convex knickpoints that dissect the middle Miocene Maya surface. They represent the front of an erosion wave that formed in response to the initial uplift of the SC range at 12 Ma. These knickpoints may have nucleated near the base of the range, along the Polochic fault, which represented the boundary between the SC range and the foreland from 12 to 7 Ma (Fig. 16a). The second cluster consists of convex knickpoints located 500 m farther down the northern flank of the SC range (Fig. 8b and 12a2). These knickpoints have heights of 200-300 m (Fig. S4-3). Assuming that this represents the amount of stream incision associated to their passage, the this passage must predate 7 Ma, because rivers have only incised 20-90 m over the past 7 My between these knickpoints and the northern front of the SC range (Brocard et al., 2011). Like the upper knickpoints, therefore, they could have nucleated on the Polochic fault. $^{10}$Be hillslope erosion rates however suggest that these two generations of knickpoints migrate very slowly today. Indeed, hillslope erosion rates should increase across upstream-migrating knickpoints in the downstream direction. Faster migrating knickpoints should geometrically promote larger differences in hillslope erosion between upstream and downstream areas (Brocard et al., 2016b). Either marginal (e.g. catchments XEU to Cub) to negligible (e.g. SMS to SMM) increase in erosion rate is documented across these knickpoints (see section 4.2), suggesting that they have stalled. Knickpoint celerity is influenced by top-down processes, such as the amount of water runoff and sediment discharge delivered from upslope (Crosby and Whipple, 2006; Brocard et al., 2016b)., and under certain circumstances, it can be influenced by bottom-up processes, such as the rate of base level fall (Whittaker and Boulton, 2012). Therefore, both the stability of the base level around the SC range over the past 7 My, and the reduction in rainfall resulting from the rise of the AC range may have contributed, together with decreasing upstream drainage area, to the slowing down of migrating knickpoints within the SC range (Fig. 16a,b). Their migration considerably slowed down over time, through a combination of (Crosby and Whipple, 2006), and of aridification in the SC range (Fig.16b).

The third cluster of knickpoints is located along the base of the mountain. It consists of concave-up knickpoints located at the apex of the pediments that have developed along the range (Fig. 8b and 12a2). These pediments are currently extensively buried under pumice deposited during a large, late Pleistocene eruption (Brocard and Morán, 2014; Rose et al., 1987). Pediments usually form under semi-arid climates, along drainages with stable base levels; they grow by their apex, in the upstream direction (Pelletier, 2010; Strudley et al., 2006; Thomas, 1989). The pediment of the SC range have developed in an area that has been incising slowly over the past 7 My (<30 m·My-1) in an area where climate is among the driest in Guatemala (Machorro, 2014), over slate, schists, gneisses, and granite. The concave-up migrating knickpoint located at the apexes of these pediments can be regarded as knickpoints that spearhead a wave of decreased incision (Baldwin, 2003). Streambed analysis further shows that these knickpoints are located at the transition between detachment-limited and transport-limited reaches downstream (Fig. S4-3) as predicted by theory (Whipple and Tucker, 2002). Lateral planation tend to dominate over vertical incision, downstream of that transition (Brocard and Van der Beek, 2006), which is also consistent with pediment development downstream. The fact that these concave-up knickpoints are located downstream of the steepest river reaches, downstream of the cluster of convex-up knickpoint located halfway the mountain side may not be coincidental, and could in fact imply that the second cluster of knickpoints did not nucleate, as hypothesized above at the front of the range. Rather, they has formed and grown in height and steepness progressively inside the range, ahead of the pediment apexes, rather than through nucleation along the Polochic fault. They would grow due to faster backwearing of the lower slopes than downwearing of the upper slopes, thus generating the steepest river reaches immediately upstream of the pediments. From a conceptual point of view, the river reaches located between the mid-flank convex knickpoints and the basal concave knickpoints can be viewed as the lips and toes of large knickzones (or knickpoint faces (Gardner, 1983)). Models predict that, if water discharge has larger influence than river gradient on stream incision, such knickpoint faces steepen and amplify over time during backwearing (Weissel and Seidl, 1998; Tucker and Whipple, 2002). This intermediate cluster is not found farther east, along the wet flank of the SM range, where no pediments have formed at the base of the range (Fig. 12d, 16c). There, only one cluster of large migrating knickpoints separates the very flat uplands of the SM range from its deeply incised, wet lower flank (Fig. 8d). The aridification, therefore, appears to be responsible to the development of stepped topography.

**5.3.3. Range-hopping erosion and the development of dry orogen interiors**

The evolution of the study area can be summarized as follows. Orogenesis started with the rise and coeval incision of the SC-SM range, from 12 to 7 Ma (Fig.16a). After 7 Ma, rock uplift decreased in the SC range while the AC range started to rise in its northern foreland. Fast uplift in the SC range led to the tectonic defeat of many rivers which, upon exiting the SC range, flowed across the foreland. Most of the defeated rivers were rerouted into the drainage of the Chixóy River, one the four rivers that maintained a course across the AC range. Transient steepening of these range-transverse rivers in response to the fast rise of the AC range and lengthening of these same rivers along the Polochic fault promoted surface uplift within the SC range. The complete cessation of river incision along the northern side of the range may therefore result from a combination of river steepening, river lengthening, and from the decrease in rock uplift rates with the SC range. However, the fact the stalling of incision is as complete along the southern side of the range as along the northern side suggest that tectonics was not the only cause, but that the aridification of the SC range, resulting from the rise of the AC range, was also instrumental in the stalling of river incision. The decrease in precipitation over the SC range reduced erosion on its hillslopes, decreased river discharge, and therefore contributed to the stalling of river incision on both sides of the range. Precipitation and erosion concentrated on the northern flanks of the AC and SM ranges, while the SC range was becoming almost passively uplifted.

The high erosion rates and wet slopes that characterize the AC range today are therefore reminiscent of the SC range from 12 to 7 Ma. The AC range has become the range that intercepts the moisture rising from foreland, while the SC has become a range located upstream, in its rain shadow. As such, it displays traits of dry orogen interior ranges and orogenic plateaus: it erodes slowly and undergoes a progressive topographic decay, marked here by the development of pediments along its base. Pediment development is promoted by a combination of aridity and of very low incision rates. Low incision rates that result from a combination of aridification in the rain shadow of frontal ranges, and of tectonic steepening of river gradients across the front ranges, is expected to characterized the growth of orogenic plateaus forming by lateral accretion (Sobel et al., 2003; Garcia-Castellanos, 2007). In the case of orogenic plateaus, however, the combination of decreased precipitation and rise of new frontal ranges achieve the disintegration of drainages, isolating dry interior drainages from the drainage of front ranges. River incision along interior drainage is reduced by the high-elevation base level maintained in the endohreic catchments. The reduction in local relief over then combines a continuation of pre-existing trends in topographic decay and pedimentation, and an added contribution of progressive sediment infilling of the now closed catchments (Sobel et al., 2003). The drying of the SC range could evolve –or not- toward full drainage disintegration.

Continued extension of the pediment and their coalescence could lead to the formation of an intramontane pediplain (Baulig, 1957), at elevations of 0.9-1.2 km, halfway between the high-standing remnants of the middle Miocene Maya surface, and the Petén-Yucatán lowlands. The Central American Dry Corridor, which straddle the SC range, continues to the NW over the Central Depression of Chiapas (Fig.1a), where more extensive pediments have developed over the basement of

the Sierra Madre de Chiapas (Authemayou et al., 2011a), in an area isolated from the Pacific moisture by the Sierra Madre de Chiapas to the SE, and from Caribbean moisture by the Sierra de Chiapas in the NW (Fig.1a). These pediments are in a more advanced process of coalescence and pediplain. The formation of such pediplains, in a context of active orogenesis may explain the great abundance of low-relief perched surfaces that appear to have form in many orogens, without significant pauses in mountain building (Calvet et al., 2015; Pain and Ollier, 1995; Babault et al., 2005).

## 6. Conclusions

- Radiometric $^{39}Ar$-$^{40}Ar$ dating on volcanic rocks confirms our earlier finding that the mountains range the closest to the plate boundary (the SM-SC range) was mostly incised during the late Miocene, from 12 to 7 Ma. Incision almost completely stalled afterwards, during the formation of the Altos de Cuchumatanes (AC r ange), farther north.

- The deformation of paleovalleys indicates that the AC range experienced > 1,000 m of uplift relative to the SC range over the past 7 My. Today the range is highly dissected. High river profile steepness and ever-expanding ice-caps indicate that the AC range still undergo fast rock and surface uplift.

- The concentration of detrital terrestrial $^{10}Be$ in the sediments of rivers that drain these ranges show that hillslope y reach 300 $m \cdot My^{-1}$ in the AC range, but are commonly <100 $\cdot My^{-1}$ in the SC-SM range. The patterns of hillslope erosion rates therefore mimic the spatial patterns of precipitation and stream incision.

- Precipitation is strongly controlled by topographic obstructions resulting from the rise of the AC range, which intercepts Caribbean moisture. Precipitation is high along the northern flanks of the AC range, but low over the SC range, which lies within rain shadows. Fossil vegetation preserved at the base of the SC range indicates a wetter climate at 7 Ma, when the AC range started to grow.

- In this context, the slow current hillslope erosion rates in the SC range appear to be contributed in part by the rise of the AC and by the development of rain shadows. It can be hypothesized, therefore, that hillslope erosion rates in the SC range were higher before the uplift of the AC range. Aridification may have also contributed to the decrease in river incision rates over the SC range.

- The rise of the AC range led to the steepening of river profiles along the rivers that maintained a course across the rising range. The steepening of river profiles triggered a transient decrease in river incision rates upstream of the AC range. The lack of resumption of river incision upstream of the AC range implies either that these rivers have not re-established equilibrium profiles, or that other factors prevent the return of incision. Aridification and river lengthening are the most likely contributors.

- The rise of the AC range indeed led to the entrenchment of range-transverse rivers along the Polochic strike-slip fault. Fault slip has driven continuous lengthening of river courses on top of the fault over the past 7 My. Lengthening contributes to the rise of river profiles upstream of the Polochic fault, and therefore to the slowing down of river incision in the SC range.

- In the SC range hillslope erosion slightly outpaces base level lowering, implying an overall trend to slow topographic decay, despite continuing surface uplift. The persistence of Middle Miocene low-relief surfaces on mountain tops in the SC range however implies no net reduction in the range height, and a decay that proceeds by backwearing rather than downwearing.

- The slowing down or erosion rates over the SC range has resulted in a slowing down and stacking of upstream-migrating knickpoints and erosion waves over the SC range and of the development of pediments at its base.

**Author contribution**

Gilles Brocard: project design, river $^{10}$Be sampling (AC and SM ranges), $^{10}$Be sample processing (AC and SM ranges), river segment analysis, manuscript preparation, with contributions from all authors. Jane Willenbring: $^{10}$Be sample processing (SM-SC range). Tristan Salles: river profile segmentation. Mickael Cosca: $^{40}$Ar/$^{39}$Ar dating. Axel Guttiérez- and Noé Cacao-Chiquín: $^{10}$Be stream sampling (SM-SC range). Sergio Morán-Ical: field work coordination. Christian Teyssier: project design and coordination.

Competing interests: The authors declare that they have no conflict of interest.

Code/Data availability: all in supplements

**Aknowledgments**

This work was supported by the Department of Geology and Geophysics at the University of Minnesota, Minneapolis, UMN grant-in-aid 1003-524-5983, and by the Swiss National Science Foundation grant 200020-120117/1.

## References


Anderson, T. H., Burkart, B., Clemons, R. E., Bohnenbe.Oh, and Blount, D. N.: Geology of the Western Altos de Cuchumatanes, Northwestern Guatemala Geological Society of America Bulletin, 84, 805-826, 10.1130/0016-7606(1973)84<805:gotwac>2.0.co;2, 1973.

Attal, M., Tucker, G. E., Whittaker, A. C., Cowie, P. A., and Roberts, G. P.: Modeling fluvial incision and transient landscape evolution: Influence of dynamic channel adjustment, Journal of Geophysical Research, 113, 10.1029/2007jf000893, 2008.

Authemayou, C., Brocard, G., Teyssier, C., Simon-Labric, T., Guttierrez, A., Chiquin, E. N., and Moran, S.: The Caribbean-North America-Cocos Triple Junction and the dynamics of the Polochic-Motagua fault systems: Pull-up and zipper models, Tectonics, 30, 10.1029/2010tc002814, 2011a.

Authemayou, C., Brocard, G., Teyssier, C., Simon-Labric, T., Guttiérrez, A., Chiquín, E., and Morán, S.: The Caribbean–North America–Cocos Triple Junction and the dynamics of the Polochic–Motagua fault systems: Pull-up and zipper models, Tectonics, 30, 2011b.

Authemayou, C., Brocard, G., Teyssier, C., Suski, B., Cosenza, B., Moran-Ical, S., Gonzalez-Veliz, C. W., Aguilar-Hengstenberg, M. A., and Holliger, K.: Quaternary seismo-tectonic activity of the Polochic Fault, Guatemala, Journal of Geophysical Research-Solid Earth, 117, 10.1029/2012jb009444, 2012.

Babault, J., Van Den Driessche, J., Bonnet, S., Castelltort, S., and Crave, A.: Origin of the highly elevated Pyrenean peneplain, Tectonics, 24, 2005.

Baldwin, J. A.: Implications of the shear stress river incision model for the timescale of postorogenic decay of topography, Journal of Geophysical Research, 108, 10.1029/2001jb000550, 2003.

Bartole, R., Lodolo, E., Obrist-Farner, J., and Morelli, D.: Sedimentary architecture, structural setting, and Late Cenozoic depocentre migration of an asymmetric transtensional basin: Lake Izabal, eastern Guatemala, Tectonophysics, 750, 419-433, 2019.

Baulig, H.: Peneplains and pediplains, Geological Society of America Bulletin, 68, 913-930, 1957.

Beaumont, C., Fullsack, P., and Hamilton, J.: Erosional control of active compressional orogens, in: Thrust tectonics, Springer, 1-18, 1992.

Bosc, E.: Geology of the San Agustin Acasaguastlan Quadrangle and Northeastern part of El Progresso Quadrangle, Guatemala, PhD thesis, Rice Univ., Houston, 1971a.

Bosc, E. A.: Geology of the San Agustin Acasaguastlan quadrangle and northeastern part of El Progreso quadrangle Rice University, 131 pp., 1971b.

Brocard, G., and Van der Beek, P.: Influence of incision rate, rock strength, and bedload supply on bedrock river gradients and valley-flat widths: Field-based evidence and calibrations from western Alpine rivers (southeast France), S. D. Willett et al., Spec. Pap. Geol. Soc. Am, 398, 101-126, 2006.

Brocard, G., Teyssier, C., Dunlap, W. J., Authemayou, C., Simon-Labric, T., Cacao-Chiquin, E. N., Gutierrez-Orrego, A., and Moran-Ical, S.: Reorganization of a deeply incised drainage: role of deformation, sedimentation and groundwater flow, Basin Research, 23, 631-651, 10.1111/j.1365-2117.2011.00510.x, 2011.

Brocard, G., Willenbring, J., Suski, B., Audra, P., Authemayou, C., Cosenza-Muralles, B., Moran-Ical, S., Demory, F., Rochette, P., Vennemann, T., Holliger, K., and Teyssier, C.: Rate and processes of river network rearrangement during incipient faulting: The case of the cahabon river, guatemala, American Journal of Science, 312, 449-507, 10.2475/05.2012.01, 2012.

Brocard, G., and Morán, S.: Phreatic clastic dikes and other degasing structures in the Los Chocoyos pumice formation, Guatemala, Revista Guatemalteca de Ciencias de la Tierra, 1, 55-65, 2014.

Brocard, G., Morán, S., Dura, T., and Vásquez, O.: The Plio-Pleistocene lacustrine Jolom Naj Formation of Cobán, Alta Verapaz: implications for the growth and demise of the Cahabón River network, Guatemala, Revista Guatemalteca de Ciencias de la Tierra, 2, 45-56, 2015a.

Brocard, G., Morán, S., Jared Vasquez, O., and Fernandez, M.: Natural hazard associated with the genesis of Lake Chichoy, Alta Verapaz, Guatemala, Revista Guatemalteca de Ciencias de la Tierra, 3, 5-19, 2016a.

Brocard, G. Y., Willenbring, J. K., Scatena, F. N., and Johnson, A. H.: Effects of a tectonically-triggered wave of incision on riverine exports and soil mineralogy in the Luquillo Mountains of Puerto Rico, Applied Geochemistry, 63, 586-598, 2015b.

Brocard, G. Y., Willenbring, J. K., Miller, T. E., and Scatena, F. N.: Relict landscape resistance to dissection by upstream migrating knickpoints, Journal of Geophysical Research: Earth Surface, 121, 1182-1203, 2016b.

Brown, E., Stallard, R. F., Larsen, M. C., Raisbeck, G. M., and Yiou, F.: Denudation rates determined from the accumulation of in-situ produced Be-10 in the Luquillo experimental forest, Puerto Rico.
, Earth and Planetary Science Letters, 129, 193-202, 10.1016/0012-821x(94)00249-x, 1995.

Bucknam, R. C., Coe, J. A., Chavarría, M. M., Godt, J. W., Tarr, A. C., Bradley, L.-A., Rafferty, S., Hancock, D., Dart, R. L., and Johnson, M. L.: Landslides triggered by Hurricane Mitch in Guatemala–inventory and discussion, US Geological Survey Open File Report, 1, 2001.

Burkart, B.: Offset across the Polochic fault of Guatemela and Chiapas, Mexico Geology, 6, 328-332, 10.1130/0091-7613(1978)6<328:oatpfo>2.0.co;2, 1978.

Callahan, R. P., Ferrier, K. L., Dixon, J., Dosseto, A., Hahm, W. J., Jessup, B. S., Miller, S. N., Hunsaker, C. T., Johnson, D. W., and Sklar, L. S.: Arrested development: Erosional equilibrium in the southern Sierra Nevada, California, maintained by feedbacks between channel incision and hillslope sediment production, GSA Bulletin, 131, 1179-1202, 2019.

Calvet, M., Gunnell, Y., and Farines, B.: Flat-topped mountain ranges: Their global distribution and value for understanding the evolution of mountain topography, Geomorphology, 241, 255-291, 2015.

Carballo-Hernandez, M., Banks, N., Franco-Austin, J., and Lopez-Aguilar, L.: Cuenca Amatique, Guatemala: Una Cuenca Transtencional al Sur del Limite de Placas NorteAmericana–Caribe, Paper Presented at Congreso Geologico Chileno, 1988,

Champel, B., van der Beek, P., Mugnier, J. L., and Leturmy, P.: Growth and lateral propagation of fault-related folds in the Siwaliks of western Nepal: Rates, mechanisms, and geomorphic signature, Journal of Geophysical Research-Solid Earth, 107, 10.1029/2001jb000578, 2002.

Clarke, B. A., and Burbank, D. W.: Bedrock fracturing, threshold hillslopes, and limits to the magnitude of bedrock landslides, Earth and Planetary Science Letters, 297, 577-586, 10.1016/j.epsl.2010.07.011, 2010.

Cowie, P. A., Whittaker, A. C., Attal, M., Roberts, G., Tucker, G. E., and Ganas, A.: New constraints on sediment-flux-dependent river incision: Implications for extracting tectonic signals from river profiles, Geology, 36, 535-538, 10.1130/g24681a.1, 2008.

Crosby, B. T., and Whipple, K. X.: Knickpoint initiation and distribution within fluvial networks: 236 waterfalls in the Waipaoa River, North Island, New Zealand, Geomorphology, 82, 16-38, 10.1016/j.geomorph.2005.08.023, 2006.

Deaton, B. C., and Burkart, B.: Time of sinistral slip along the Polochic fault of Guatemala Tectonophysics, 102, 297-&, 10.1016/0040-1951(84)90018-0, 1984.

Ferrier, K. L., Kirchner, J. W., Riebe, C. S., and Finkel, R. C.: Mineral-specific chemical weathering rates over millennial timescales: Measurements at Rio Icacos, Puerto Rico, Chemical Geology, 277, 101-114, 10.1016/j.chemgeo.2010.07.013, 2010.

Ferrier, K. L., Perron, J. T., Mukhopadhyay, S., Rosener, M., Stock, J. D., Huppert, K. L., and Slosberg, M.: Covariation of climate and long-term erosion rates across a steep rainfall gradient on the Hawaiian island of Kaua ‘i, Geological Society of America Bulletin, 125, 1146-1163, 2013.

Finnegan, N. J., Hallet, B., Montgomery, D. R., Zeitler, P. K., Stone, J. O., Anders, A. M., and Yuping, L.: Coupling of rock uplift and river incision in the Namche Barwa-Gyala Peri massif, Tibet, Geological Society of America Bulletin, 120, 142-155, 10.1130/b26224.1, 2008.

Flores, K. E., Martens, U. C., Harlow, G. E., Brueckner, H. K., and Pearson, N. J.: Jadeitite formed during subduction: In situ zircon geochronology constraints from two different tectonic events within the Guatemala Suture Zone, Earth and Planetary Science Letters, 371-372, 67-81, 10.1016/j.epsl.2013.04.015, 2013.

Galewsky, J.: Rain shadow development during the growth of mountain ranges: An atmospheric dynamics perspective, Journal of Geophysical Research: Earth Surface, 114, 2009.

Garcia-Castellanos, D.: The role of climate during high plateau formation. Insights from numerical experiments, Earth and Planetary Science Letters, 257, 372-390, 2007.

Gardner, T. W.: Experimental study of knickpoint and longitudinal profile evolution in cohesive, homogeneous material, Geological Society of America Bulletin, 94, 664, 10.1130/0016-7606(1983)94<664:esokal>2.0.co;2, 1983.

Goldrick, G., and Bishop, P.: Differentiating the roles of lithology and uplift in the steepening of bedrock river long profiles: an example from southeastern Australia, The Journal of Geology, 103, 227-231, 1995.

Gould, W. A., Alarcón, C., Fevold, B., Jiménez, M. E., Martinuzzi, S., Potts, G., Quiñones, M., Solórzano, M., and Ventosa, E.: The Puerto Rico Gap Analysis Project volume 1: land cover, vertebrate species distributions, and land stewardship, Gen. Tech. Rep. IITF-39, 1, 2008.

Guttiérrez, A.: Caracterización de conglomerados y areniscas en la formación Subinal, en el suroriente del país, University San Carlos de Guatemala, 90, 2008.

Guzmán-Speziale, M.: Beyond the Motagua and Polochic faults: Active strike-slip faulting along the Western North America–Caribbean plate boundary zone, Tectonophysics, 496, 17-27, 10.1016/j.tecto.2010.10.002, 2010.

Harp, E. L., Wilson, R. C., and Wieczorek, G. F.: Landslides from the February 4, 1976, Guatemala earthquake, US Government Printing Office Washington, DC, 1981.

Harvey, A. M.: Effective timescales of coupling within fluvial systems, Geomorphology, 44, 175-201, 2002.

Hirschman, T.: Reconnaissance geology of part of the Department of El Progreso, Guatemala: Unpub, Master's thesis, Univ. Indiana, 1962.

Holder, C. D.: Rainfall interception and fog precipitation in a tropical montane cloud forest of Guatemala, Forest Ecology and Management, 190, 373-384, 10.1016/j.foreco.2003.11.004, 2004.

Howard, A. D.: A detachment-limited model of drainage basin evolution, Water resources research, 30, 2261-2285, 1994.

Howard, A. D.: Badland morphology and evolution: Interpretation using a simulation model, Earth Surface Processes and Landforms: The Journal of the British Geomorphological Group, 22, 211-227, 1997.

Humphrey, N. F., and Heller, P. L.: Natural oscillations in coupled geomorphic systems: An alternative origin for cyclic sedimentation, Geology, 23, 499, 10.1130/0091-7613(1995)023<0499:noicgs>2.3.co;2, 1995.

Jackson, J., Ritz, J. F., Siame, L., Raisbeck, G., Yiou, F., Norris, R., Youngson, J., and Bennett, E.: Fault growth and landscape development rates in Otago, New Zealand, using in situ cosmogenic Be-10, Earth and Planetary Science Letters, 195, 185-193, 10.1016/s0012-821x(01)00583-0, 2002.

Kirby, E.: Distribution of active rock uplift along the eastern margin of the Tibetan Plateau: Inferences from bedrock channel longitudinal profiles, Journal of Geophysical Research, 108, 10.1029/2001jb000861, 2003.

Lachniet, M. S., and Vazquez-Selem, L.: Last Glacial Maximum equilibrium line altitudes in the circum-Caribbean (Mexico, Guatemala, Costa Rica, Colombia, and Venezuela), Quaternary International, 138-139, 129-144, 10.1016/j.quaint.2005.02.010, 2005.

Leland, J., Reid, M. R., Burbank, D. W., Finkel, R., and Caffee, M.: Incision and differential bedrock uplift along the Indus River near Nanga Parbat, Pakistan Himalaya, from Be-10 and Al-26 exposure age dating of bedrock straths, Earth and Planetary Science Letters, 154, 93-107, 10.1016/s0012-821x(97)00171-4, 1998.

Liang, Z., Liu, H., Zhao, Y., Wang, Q., Wu, Z., Deng, L., and Gao, H.: Effects of rainfall intensity, slope angle, and vegetation coverage on the erosion characteristics of Pisha sandstone slopes under simulated rainfall conditions, Environmental Science and Pollution Research, 1-10, 2019.

Machorro, R. C., S.: Drought assessment in the Dry Corridor of Guatemala, Earth Science Review of Guatemala, 1, 11, 2014.

McAdams, B. C., Trierweiler, A. M., Welch, S. A., Restrepo, C., and Carey, A. E.: Two sides to every range: orographic influences on CO 2 consumption by silicate weathering, Applied Geochemistry, 63, 472-483, 2015.

Meijers, M., Brocard, G., Lüdecke, T., Cosca, M., Teyssier, C., Whitney, D., and Mulch, A.: Rapid Late Miocene Surface Uplift of the Central Anatolian Plateau Margin., Earth and Planetary Research Letters, 2018.

Merritts, D. J., Vincent, K. R., and Wohl, E. E.: LONG RIVER PROFILES, TECTONISM, AND EUSTASY - A GUIDE TO INTERPRETING FLUXIAL TERRACES, Journal of Geophysical Research-Solid Earth, 99, 14031-14050, 10.1029/94jb00857, 1994.

Montgomery, D. R., and Stolar, D. B.: Reconsidering Himalayan river anticlines, Geomorphology, 82, 4-15, 10.1016/j.geomorph.2005.08.021, 2006.

Mudd, S. M., and Furbish, D. J.: Responses of soil-mantled hillslopes to transient channel incision rates, Journal of Geophysical Research: Earth Surface, 112, 2007.

Mudd, S. M., Attal, M., Milodowski, D. T., Grieve, S. W., and Valters, D. A.: A statistical framework to quantify spatial variation in channel gradients using the integral method of channel profile analysis, Journal of Geophysical Research: Earth Surface, 119, 138-152, 2014.

Muller, P. D.: Geology of the Los Amates quadrangle and vicinity, Guatemala, Central America, State University of NY, 1979.

Murphy, B. P., Johnson, J. P., Gasparini, N. M., and Sklar, L. S.: Chemical weathering as a mechanism for the climatic control of bedrock river incision, Nature, 532, 223, 2016.

Neely, A. B., and DiBiase, R. A.: Drainage Area, Bedrock Fracture Spacing, and Weathering Controls on Landscape-Scale Patterns in Surface Sediment Grain Size, Journal of Geophysical Research: Earth Surface, 125, e2020JF005560, 2020.

Newcomb, W. E.: Geology, Structure and Metamorphism of the Chuacus Group, Rio Hondo Quadrangle and Vicinity, Guatemala, State University of New York at Binghamton, 1975.

Ortega-Gutierrez, F., Solari, L. A., Sole, J., Martens, U., Gomez-Tuena, A., Moran-Ical, S., Reyes-Salas, M., and Ortega-Obregon, C.: Polyphase, high-temperature eclogite-facies metamorphism in the Chuacus Complex, Central Guatemala: Petrology, geochronology, and tectonic implications, International Geology Review, 46, 445-470, 10.2747/0020-6814.46.5.445, 2004.

Ortega-Obregón, C., Solari, L., Keppie, J., Ortega-Gutiérrez, F., Solé, J., and Morán-Ical, S.: Middle-Late Ordovician magmatism and Late Cretaceous collision in the southern Maya block, Rabinal-Salamá area, central Guatemala: implications for North America–Caribbean plate tectonics, Geological Society of America Bulletin, 120, 556-570, 2008.

Pain, C., and Ollier, C.: Inversion of relief—a component of landscape evolution, Geomorphology, 12, 151-165, 1995.

Pelletier, J. D.: How do pediments form?: A numerical modeling investigation with comparison to pediments in southern Arizona, USA, Geological Society of America Bulletin, 122, 1815-1829, 10.1130/b30128.1, 2010.

Perron, J. T., and Royden, L.: An integral approach to bedrock river profile analysis, Earth Surface Processes and Landforms, 38, 570-576, 10.1002/esp.3302, 2013.

Ramos Scharrón, C. E., Castellanos, E. J., and Restrepo, C.: The transfer of modern organic carbon by landslide activity in tropical montane ecosystems, Journal of Geophysical Research, 117, 10.1029/2011jg001838, 2012.

Ratschbacher, L., Franz, L., Min, M., Bachmann, R., Martens, U., Stanek, K., Stubner, K., Nelson, B. K., Herrmann, U., Weber, B., Lopez-Martinez, M., Jonckheere, R., Sperner, B., Tichomirowa, M., McWilliams, M. O., Gordon, M., Meschede, M., and Bock, P.: The North American-Caribbean Plate boundary in Mexico-Guatemala-Honduras, Geological Society, London, Special Publications, 328, 219-293, 10.1144/sp328.11, 2009.

Riebe, C. S., Sklar, L. S., Lukens, C. E., and Shuster, D. L.: Climate and topography control the size and flux of sediment produced on steep mountain slopes, Proceedings of the National Academy of Sciences, 112, 15574-15579, 2015.

Rogers, R. D., and Mann, P.: Transtensional deformation of the western Caribbean–North America plate boundary zone, Geological Society of America Special Papers, 428, 37-64, 2007.

Roper, P.: Stratigraphy of the Chuacu¤ s Group on the south side of the Sierra de las Minas range, Guatemala, Geol. Mijn, 57, 309-313, 1978.

Rose, W. I., Newhall, C. G., Bornhorst, T. J., and Self, S.: Quaternary silicic pyroclastic deposits of atitlan caldera, Guatemala, Journal of Volcanology and Geothermal Research, 33, 57-80, 10.1016/0377-0273(87)90054-0, 1987.

Rosenbloom, N. A., and Anderson, R. S.: Hillslope and channel evolution in a marine terraced landscape, Santa Cruz, California, Journal of Geophysical Research: Solid Earth, 99, 14013-14029, 1994.

Royden, L., and Taylor Perron, J.: Solutions of the stream power equation and application to the evolution of river longitudinal profiles, Journal of Geophysical Research: Earth Surface, 118, 497-518, 2013.

Sieh, K. E., and Jahns, R. H.: Holocene activity of the San Andreas fault at Wallace Creek, California, Geological Society of America Bulletin, 95, 883, 10.1130/0016-7606(1984)95<883:haotsa>2.0.co;2, 1984.

Simon-Labric, T., Brocard, G. Y., Teyssier, C., van der Beek, P. A., Fellin, M. G., Reiners, P. W., and Authemayou, C.: Preservation of contrasting geothermal gradients across the Caribbean-North America plate boundary (Motagua Fault, Guatemala), Tectonics, n/a-n/a, 10.1002/tect.20060, 2013.

Sklar, L. S., and Dietrich, W. E.: The role of sediment in controlling steady-state bedrock channel slope: Implications of the saltation–abrasion incision model, Geomorphology, 82, 58-83, 10.1016/j.geomorph.2005.08.019, 2006.

Sobel, E. R., Hilley, G. E., and Strecker, M. R.: Formation of internally drained contractional basins by aridity-limited bedrock incision, Journal of Geophysical Research: Solid Earth, 108, 2003.

Strudley, M. W., Murray, A. B., and Haff, P. K.: Emergence of pediments, tors, and piedmont junctions from a bedrock weathering–regolith thickness feedback, Geology, 34, 805, 10.1130/g22482.1, 2006.

Thattai, D., Kjerfve, B., and Heyman, W.: Hydrometeorology and variability of water discharge and sediment load in the inner Gulf of Honduras, western Caribbean, Journal of Hydrometeorology, 4, 985-995, 2003.

Thomas, M. F.: The role of etch processes in landform development. I. Etching concepts and their applications, Zeitschrift für Geomorphologie, 33, 129-142, 1989.

Tobisch, M. K.: Part I, late Cenozoic geology of the central Motagua Valley, Guatemala: part II, uplift rates, deformation and neotectonics of Holocene marine terraces from Point Delgado to Cape Mendocino, California, 1986.

Tucker, G. E., and Whipple, K.: Topographic outcomes predicted by stream erosion models: Sensitivity analysis and intermodel comparison, Journal of Geophysical Research, 107, 10.1029/2001jb000162, 2002.

van der Beek, P., Champel, B., and Mugnier, J. L.: Control of detachment dip on drainage development in regions of active fault-propagation folding, Geology, 30, 471-474, 10.1130/0091-7613(2002)030<0471:coddod>2.0.co;2, 2002.

Weissel, J. K., and Seidl, M. A.: Inland propagation of erosional escarpments and river profile evolution across the southeast Australian passive continental margin, Rivers over rock: fluvial processes in bedrock channels, 189-206, 1998.

Whipple, K., and Meade, B.: Orogen response to changes in climatic and tectonic forcing, Earth and Planetary Science Letters, 243, 218-228, 10.1016/j.epsl.2005.12.022, 2006.

Whipple, K. X., and Tucker, G. E.: Dynamics of the stream-power river incision model: Implications for height limits of mountain ranges, landscape response timescales, and research needs, Journal of Geophysical Research, 104, 17661, 10.1029/1999jb900120, 1999.

Whipple, K. X., and Tucker, G. E.: Implications of sediment-flux-dependent river incision models for landscape evolution, Journal of Geophysical Research-Solid Earth, 107, 10.1029/2000jb000044, 2002.

Whipple, K. X.: Bedrock rivers and the geomorphology of active orogens, Annu. Rev. Earth Planet. Sci., 32, 151-185, 2004.

Whittaker, A. C., and Boulton, S. J.: Tectonic and climatic controls on knickpoint retreat rates and landscape response times, Journal of Geophysical Research, 117, 10.1029/2011jf002157, 2012.

Willenbring, J. K., Codilean, A. T., and McElroy, B.: Earth is (mostly) flat: Apportionment of the flux of continental sediment over millennial time scales, Geology, 41, 343-346, 10.1130/g33918.1, 2013a.

Willenbring, J. K., Gasparini, N. M., Crosby, B. T., and Brocard, G.: What does a mean mean? The temporal evolution of detrital cosmogenic denudation rates in a transient landscape, Geology, 41, 1215-1218, 2013b.

Willett, S. D., and Brandon, M. T.: On steady states in mountain belts, Geology, 30, 175, 10.1130/0091-7613(2002)030<0175:ossimb>2.0.co;2, 2002.

Williams, E. A., and McBirney, A. R.: Volcanic history of Honduras, University of California publications in Geological Sciences, 85, 1-65, 1969.